



Contents lists available at ScienceDirect

## Geochimica et Cosmochimica Acta

journal homepage: [www.elsevier.com/locate/gca](http://www.elsevier.com/locate/gca)

## Cold-subduction biogeodynamics boosts deep energy delivery to the forearc

Veronica Peverelli<sup>a,\*</sup>, Orlando Sébastien Olivieri<sup>a</sup>, Tatsuki Tsujimori<sup>b,c</sup>,  
Donato Giovannelli<sup>d,e,f,g,h</sup>, Guanghai Shi<sup>i</sup>, Enrico Cannà<sup>j</sup>, Francesca Piccoli<sup>k</sup>,  
Alberto Vitale Brovarone<sup>a,l,m</sup>

<sup>a</sup> Department of Biological, Geological and Environmental Sciences, Università degli Studi di Bologna, Bologna, Italy<sup>b</sup> Center for Northeast Asian Studies, Tohoku University, Sendai 980-8578, Japan<sup>c</sup> Department of Earth Science, Graduate School of Science, Tohoku University, Sendai 980-8578, Japan<sup>d</sup> Department of Biology, University of Naples Federico II, Naples, Italy<sup>e</sup> Institute for Marine Biological Resources and Biotechnologies, Italian National Research Council, CNR-IRBIM, Ancona, Italy<sup>f</sup> Earth-Life Science Institute, ELSI, Tokyo Institute of Technology, Tokyo, Japan<sup>g</sup> Marine Chemistry and Geochemistry Department, Woods Hole Oceanographic Institution, Woods Hole, MA, USA<sup>h</sup> Department of Marine and Coastal Science, Rutgers University, New Brunswick, NJ, USA<sup>i</sup> School of Gemology, China University of Geosciences, Beijing 100083, China<sup>j</sup> Dipartimento di Scienze della Terra "A. Desio", Università degli Studi di Milano - La Statale, Milano, Italy<sup>k</sup> Institute of Geological Sciences, University of Bern, Bern, Switzerland<sup>l</sup> Institut de Minéralogie, de Physique des Matériaux et de Cosmochimie (IMPMC), Sorbonne Université, Muséum National d'Histoire Naturelle, UMR CNRS 7590, IRD UR206, 75005 Paris, France<sup>m</sup> Institute of Geosciences and Earth Resources, National Research Council of Italy, Pisa, Italy

## ARTICLE INFO

Associate editor: Ralf Halama

## Keywords:

Plate interface  
Metasomatic rocks  
Reduced energy sources  
Subsurface microbial life  
Biogeodynamics

## ABSTRACT

Metamorphic fluids in subduction zones carry C–H–N–O–P–S species, which are crucial for sustaining subsurface microbial life at shallower crustal depths in the forearc region. Upwards migration of deeply released fluids to shallower levels, where temperatures permit the persistence of microbial life, is recorded by metasomatic rocks formed along the plate interface. Variations in the redox state and component speciation of metamorphic fluids – from local to secular, and highly dependent on thermal gradients and redox state of subduction inputs – may strongly control microbial pathways or even the possibility for metamorphic fluids to sustain microbial communities in the subsurface biosphere at convergent plate margins. We show that metamorphic fluids containing reduced energy sources for microbial life – e.g., CH<sub>4</sub>, H<sub>2</sub> – are common in Phanerozoic, high-pressure/low-temperature plate-interface metasomatic rocks such as jadeitites and albitites worldwide. Based on the stability fields of minerals hosting CH<sub>4</sub>, H<sub>2</sub> and graphite inclusions, we pinpoint the protracted, probably episodic migration of energy sources in the mantle wedge via fluid circulation being mediated by jadeitites from > ca. 35 km depth, and by their retrogressed counterparts forming from between 35–15 km depth. These fluids can cross the so-called biotic fringe – whose limit is the depth corresponding to ca. 122–135 °C (as deep as ca. 13 km depth depending on geothermal gradients) – as suggested by previous documentation of slab-derived fluids reaching subsurface microbial communities. Thermodynamic modeling indicates that cool thermal gradients, possibly combined with increased inputs of organic matter-rich sediments into subduction, favor the abundance of reduced energy sources relative to more oxidized species (e.g., CO<sub>2</sub>), thus promoting the proliferation of subsurface microbial life at convergent margins.

## 1. Introduction

The interplay of geological and microbiological processes accompanying chemical cycling at convergent margins is a fundamental

component of biogeodynamics (e.g., Zerkle, 2018; Giuliani et al., 2022), and has marked key steps in Earth's evolution (e.g., Hazen et al., 2008). Although the persistence of microbial life in the lithosphere is limited to levels shallower than the depth corresponding to maximum ca. 122–135

\* Corresponding author.

E-mail address: [veronica.peverelli2@unibo.it](mailto:veronica.peverelli2@unibo.it) (V. Peverelli).<https://doi.org/10.1016/j.gca.2024.10.004>

Received 7 July 2024; Accepted 4 October 2024

Available online 6 October 2024

0016-7037/© 2024 The Authors. Published by Elsevier Ltd. This is an open access article under the CC BY license (<http://creativecommons.org/licenses/by/4.0/>).

°C (Takai et al., 2008; Heuer et al., 2020; but also higher, see Yanagawa et al., 2017), C–H–N–O–P–S fluids feeding subsurface microbial communities in the forearc region of convergent margins can be sourced from greater depths, as pointed out by direct and indirect evidence: At the Mariana forearc, energy sources such as CH<sub>4</sub> and H<sub>2</sub>, which feed subsurface microbial communities in a hydrothermal system hosted by a serpentinite mud volcano, are provided by metamorphic fluids being released at least 27 km below the seafloor (Mottl et al., 2003), but also as deep as the slab-mantle wedge interface (Ohara et al., 2012). Indirect evidence for deeply sourced carbonic fluids feeding subsurface microbial life is encountered at other convergent margins as well – e.g., Peru and the Central American Convergent Margin (Barry et al., 2019; Fullerton et al., 2021); Andes (Barry et al., 2022; Rogers et al., 2023; Upin et al., 2023) – where isotopic and microbiological data of deeply sourced hot springs point to carbon sequestration mediated by microbial chemolithoautotrophy (i.e., the conversion of inorganic carbon sources to biomass in the absence of light) within the subsurface crust.

Fluids rich in CH<sub>4</sub> and H<sub>2</sub> play an important role in microbiological processes by promoting energy-conserving microbial redox reactions. In subduction zones, such reduced metamorphic fluids can be produced in the down-going slab and in the mantle wedge at great depths through multiple processes such as metamorphism of organic matter-rich sedimentary rocks, serpentinization, as well as deserpentinization and devolatilization of carbonated mafic and ultramafic rocks if controlled by infiltration of reduced fluids (Mullis, 1979; Mullis et al., 1994; Tao et al., 2018; Piccoli et al., 2019; Vitale et al., 2020; Herviou et al., 2021; Padrón-Navarta et al., 2023; Boutier et al., 2024b; Harada and Tsujimori, 2024; Suzuki et al., 2024). Although such processes take place at depths corresponding to temperature (T) conditions that preclude microbial life (Takai et al., 2008; Plümpner et al., 2017; Vitale et al., 2020), the migration of the resulting fluids towards life-sustaining levels (i.e., shallower than the depth corresponding to 122–135 °C – the so-called biotic fringe; Takai et al., 2008; Heuer et al., 2020) would imply that large sources of energy can feed microbial life in the subsurface biosphere.

The plate interface and the metasomatic rocks forming along it are preferential fluid conduits (e.g., Harlow and Sorensen, 2005; Harlow et al., 2015; Angiboust et al., 2021b, a; Piccoli et al., 2021). Jadeitites and associated albitites are metasomatic rocks forming along the plate boundary and, in many cases, as fluid-deposited products in the mantle wedge (Tsujimori and Harlow, 2012; Harlow et al., 2015). They are found at multiple paleo-plate interfaces, but the preserved jadeite record is exclusively Phanerozoic (Harlow and Sorensen, 2005; Tsujimori and Harlow, 2012; Harlow et al., 2015). P-type (i.e., “precipitated type”) jadeitites are fluid-precipitated rocks that are mainly constituted by jadeite (NaAlSi<sub>2</sub>O<sub>6</sub>). The direct precipitation from a fluid – supported by several lines of evidence (see Harlow et al., 2015; and references therein) – distinguishes between P-type jadeitites and R-type (i.e., “replacive type”) ones, the latter forming as replacement of plagiogranites, metagabbros and eclogites (Tsujimori and Harlow, 2012). However, recent work suggests that many jadeitites considered as P-type may be replacive in nature (Angiboust et al., 2021b,a). The fluids involved in the formation of jadeitites are often interpreted as being slab-derived serpentinizing fluids based on geochemical data (Chen et al., 2023) and on their association with exhumed serpentinites (Harlow et al., 2015). Jadeitites are interpreted to form at a minimum pressure (P) of, respectively, 1 GPa (quartz-bearing) and 0.7 GPa (quartz-free) (Harlow et al., 2015). Albitites associated with jadeitites are their retrogressed counterparts, forming during exhumation of jadeite precursors when crossing the jadeite-albite boundary at ca. 35 km depth (< ca. 1 GPa) for quartz-bearing jadeitites (e.g., Harlow, 1994; Harlow and Sorensen, 2005; Tsujimori and Harlow, 2012; Harlow et al., 2015). Methane has been detected in fluid inclusions (FIs hereafter) in some jadeite localities: South Motagua Mélange in Guatemala (Harlow et al., 2015), Myanmar (Shi et al., 2005), Japan (Tsujimori and Harlow, 2017), Kazakhstan (Wen et al., 2023), New Idria (Takahashi et al.,

2017), Polar Urals in Russia (Meng et al., 2011) and the Lanzo Massif in the Western Alps, where H<sub>2</sub> was also detected in FIs (Giuntoli et al., 2024). However, the significance of CH<sub>4</sub> and other energy sources in plate-interface metasomatic rocks (such as fresh and retrogressed jadeitites) worldwide has not been assessed.

In this study, we use microstructural, geochemical, and geochronological data to investigate the circulation of CH<sub>4</sub>, H<sub>2</sub> and life-building blocks such as N species through plate-interface P-type jadeitites, albitites, and other metasomatic rocks from (paleo-)convergent plate boundaries scattered all over the world (Fig. 1). The investigated samples span ca. 400 Myr within the Phanerozoic eon and most of the known jadeitites localities worldwide.

## 2. Materials and methods

To constrain the occurrence, timing, and duration of deep energy migration along paleo-plate boundaries, we studied plate-interface metasomatic rocks from eleven localities worldwide (blue circles in Fig. 1) for petrographic and FI analyses. All jadeitites studied here are interpreted as P-type jadeitites (Tsujimori and Harlow, 2012; described in Supplement C in the Supplementary material). We inspected one jadeite sample from the North Motagua Mélange (Guatemala), one jadeite and one albitite from Osayama (Japan), jadeitites and one metasomatized granite from Itoigawa–Omi (Japan), jadeitites and one diopside from Kamuikotan/Hokkaido, and jadeitites from New Idria (USA), Myanmar, Kazakhstan, the Lanzo Massif (Western Italian Alps), and the Polar Urals, Chukotka and West Sayan (Russia; Table 1). Three samples from two localities were selected for titanite U–Pb geochronology to ascertain the protracted circulation of CH<sub>4</sub>-rich fluids along the plate interface: one fresh jadeite (sample GT1) from the North Motagua Mélange (Guatemala), and one partially retrogressed jadeite (sample OSJ1002) and one albitite (sample R5) from Osayama (Japan). These are the only samples which host sufficient titanite material for ca. 30 U–Pb spot analyses. Titanite is the chosen geochronometer for this study because, besides zircon (generally proposed to date the formation of P-type jadeitites; see Sect. 3.2), it is the only dateable mineral that hosts graphite, CH<sub>4</sub> and H<sub>2</sub> in the studied samples, it is present in more than one sample, and it is considered as a secondary phase to jadeite formation (Tsujimori and Harlow, 2012). Other geochronometers (i.e., garnet and apatite) were not analyzed because grains are too small and/or too scarce to permit the acquisition of enough datapoints for a Terrestrial–Wasserburg regression. Hence, a comparison between age of jadeite formation (if available and reliable; see Sect. 4.1) and titanite formation can reveal protracted circulation of CH<sub>4</sub> and other reduced chemical species from jadeite formation to its retrogression.

### 2.1. Petrography and fluid inclusion characterization

Descriptions of the studied samples are available in the Supplementary material (Supplement C; Figs. S19–S32). Thin sections were inspected in the laboratory facilities of the department of Biological, Geological and Environmental Sciences (BiGeA) of the University of Bologna (Italy). Transmitted-light photomicrographs were acquired on a ZEISS AxioScope 7 equipped with a ZEISS Axiocam 305 color using the ZEISS ZEN core software (version 3.6) in the DeepCarbon Lab of the BiGeA Department. Stacked images and photomicrographs were used to select FIs to be analyzed by micro-Raman spectroscopy, and to assess the presence of graphite in the samples.

Micro-Raman spectroscopy was performed at the BiGeA Department, University of Bologna (Italy), using a WITec alpha300 R system to identify chemical species in FIs in several minerals, and to obtain spectra of graphite and rock-forming minerals. The WITec alpha300 R system is equipped with a 532 nm laser. All analyses were carried out using an EC Epiplan-Neofluar 100x/0.9 DIC objective after focusing on the FI to be analyzed, or the vapor bubble therein when present. Grating was 600 gr mm<sup>-1</sup>. Variable laser power of ca. 5–35 mW was employed for FIs, with

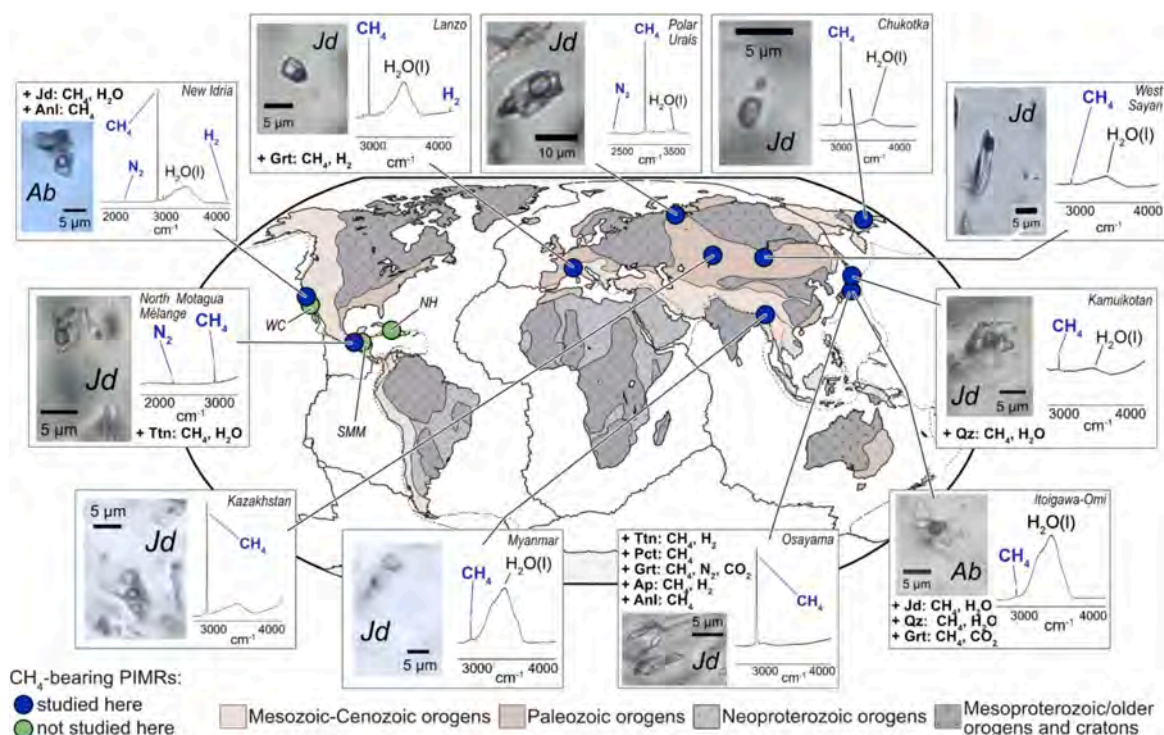


**Fig. 1.** Worldwide distribution of energy sources ( $\text{CH}_4$ ,  $\text{H}_2$ ) and other species (e.g.,  $\text{N}_2$ ) important for microbial activities in jadeitites and other associated plate-interface metasomatic rocks all around the world, with micro-Raman spectra and photomicrographs in plane-polarized light of representative fluid inclusions hosted by higher- and lower-pressure minerals (e.g., jadeite and albite, respectively). PIMRs: plate-interface metasomatic rocks; NH: Northern Hispaniola; SMM: South Motagua Mélange; WC: Ward Creek. Ab: albite; Anl: analcime; Ap: apatite; Grt: garnet; Jd: jadeite; Pct: pectolite; Qz: quartz; Ttn: titanite. The photomicrographs were acquired using the ZEISS ZEN core software (version 3.6). The base of the map is after Tsujimori and Harlow (2012). See Table 1, and the Supplementary material (Table S1) for detailed results.

integration times of 40–60 sec and 10–15 accumulations. Lower laser power was used to avoid graphite precipitating within the FIs from  $\text{CH}_4$ , then progressively increased to obtain higher-quality spectra. For graphite, laser power was ca. 3 mW during 4–6 accumulations of 20–40 sec each. Spectra of host minerals were acquired using a laser power of ca. 5 mW during 5–10 accumulations of 20 sec each. The instrument contains an Ar-Hg lamp integrated in the optical path to calibrate the Raman shift through the detection of Ar-Hg calibration lines. Where possible, the laser beam was focused on gaseous bubbles in biphasic FIs, hence producing spectra without the  $\text{H}_2\text{O}$  band of the liquid phase. Fluid inclusions smaller than a few microns, although present and sometimes dominant, could not be analyzed. Therefore, it cannot be unraveled here if any immiscibility processes produced any  $\text{CH}_4$ -rich,  $\text{H}_2\text{O}$ -free FIs (which is possible at the temperature conditions at which jadeitites form; see Johnson and Harlow, 1999), in that a sampling bias due to FI size could not be avoided. The detailed results are reported in Tables 1 and S1 and Figs. S1–S17.

## 2.2. Titanite and zircon U–Pb geochronology

Measurements of U and Pb isotope ratios for titanite U–Pb geochronology by laser ablation inductively coupled plasma mass spectrometry (LA-ICP-MS) were performed in three analytical sessions in two different laboratories. Specific conditions and parameters of each session are shown in Tables S2–S3 (Supplementary material). The analyses were carried out on thin sections that were pre-cleaned with ethanol before being placed in the sample holders. In all sessions, analytical conditions were optimized using the NIST SRM612 synthetic glass standard. The first two analytical sessions were carried out at the Geochemistry, Geochronology and Isotope Geology laboratory hosted at the Earth Sciences Department of the University of Milan (Italy, ESD-UniMi), using a 193 nm ATLEX 300 LR ultra-short pulse, compact, air-

cooled excimer laser (Analyte Excimer from Teledyne Photon Machines) coupled to a single-detector quadrupole ICP-MS iCAP RQ from Thermo Fisher Scientific. Raw data were treated in Glitter (Griffin et al., 2008). A third analytical session was performed at the University of Bern (Switzerland), which is equipped with a Resonetics RESOLUTIONSE 193 nm excimer laser system (Applied Spectra, USA) equipped with an S-155 large-volume constant-geometry chamber (Laurin Technic, Australia) coupled to an Agilent 7900 ICP-QMS. Raw data were treated using the software Iolite and the VisualAge\_Ucompbine data reduction scheme (Chew et al., 2014). The MKED1 titanite (Spandler et al., 2016) was used as primary reference material in all three analytical sessions, and several well-characterized and in-house secondary reference materials (see Tables S2–S3) were used to assess accuracy of the obtained ages (Fig. S18). U–Pb isotope ratios returned by Glitter and Iolite after data reduction are in the supplementary material (Tables S4–S5).

Measurements of U–Pb isotope data for zircon LA-ICP-MS geochronology were carried out at Okayama University of Science, Japan, by employing a Teledyne Cetac Technologies Analyte G2 ArF excimer laser ablation system equipped with a HelEx 2 vol sample chamber, coupled to a Thermo Fisher Scientific iCAP-RQ single-collector quadrupole ICP-MS. The 91500 zircon (Wiedenbeck et al., 1995, 2004) was used as the primary standard. Plešovice zircon was employed as the secondary standard for quality control and returned an age consistent with its published reference age (Fig. S18; Sláma et al., 2008). U–Pb isotope ratios used for age calculation after data reduction are in the supplementary material (Table S6).

The U–Pb isotope data used for age calculations (Tables S4–S6) are not corrected for initial Pb, as the use of Tera–Wasserburg ( $^{238}\text{U}/^{206}\text{Pb}$ – $^{207}\text{Pb}/^{206}\text{Pb}$ ) diagrams does not require initial Pb corrections. All Tera–Wasserburg diagrams (Figs. 3 and S18) are plotted using IsoplotR (Vermeesch, 2018).

**Table 1**

Data acquired on the WITec alpha300 R micro-Raman spectroscope. Fluid inclusions are classified as primary only if no relationships are observed between isolated fluid inclusions and features such as cleavage, fractures or fluid inclusion trails, if they cluster in the core of the host mineral, or if they are aligned consistently with crystal growth. A question mark is used to indicate uncertainty in whether fluid inclusions are primary or secondary. Fls = fluid inclusions; SIs = solid inclusions. The timings of jadeite formation and retrogression reported here are from Tsujimori and Harlow (2012) unless specified. The number of fluid inclusions in which each species is detected is indicated by “n = x/y”, where “y” is the total number of analyzed fluid inclusions and “x” the number in which the species is detected.

Country	Locality	Sample	Host	Chemical species	Primary/ secondary	Jadeite formation	Circulation of energy sources
Guatemala	North Motagua Mélange	GT1 ( <i>jadeite</i> ; Fig. 2a)	Jadeite	Fls: CH <sub>4</sub> , N <sub>2</sub> , H <sub>2</sub> O (all, n = 2/2) SIs: graphite	Primary? –	98–95 Ma (Yui et al., 2010)	Jadeite formation–retrogression (77–65 Ma)
			Titanite	Fls: CH <sub>4</sub> (n = 3/3) H <sub>2</sub> O (n = 1/3) SIs: graphite	Secondary –		
Japan	Osayama	OSJ1002 ( <i>jadeite</i> ; Fig. 2b)	Jadeite	Fls: CH <sub>4</sub> (n = 1/2), H <sub>2</sub> O (n = 1/2) SIs: graphite	Secondary? –	523.6 ± 3.5 Ma ( Fig. 3) Zrn U–Pb (this work)	Jadeite formation–retrogression (? Ma)
			Titanite1	–	–		
			Titanite2	SIs: graphite	–		
			Pectolite	Fls: CH <sub>4</sub> (n = 2/2)	Secondary		
			Titanite	Fls: H <sub>2</sub> (n = 3/5), CH <sub>4</sub> (n = 4/5) CO <sub>2</sub> (?; n = 2/5), NH <sub>4</sub> (?; n = 1/5) SIs: graphite	Secondary –		
			Albite	Fls: H <sub>2</sub> O (n = 1/1) SIs: graphite	Primary? –		
	Itoigawa–Omi	KYJ3-2 ( <i>jadeite</i> ; Fig. S19)	Jadeite	Fls: CH <sub>4</sub> (n = 4/4), N <sub>2</sub> (n = 1/4), H <sub>2</sub> O (n = 3/4) SIs: graphite	Primary –	ca. 520 Ma Zrn U–Pb (Kunugiza and Goto, 2010)	Jadeite formation–retrogression (ca. 350–320 Ma)
			Jadeite	Fls: CH <sub>4</sub> (n = 4/4), H <sub>2</sub> O (n = 4/4), N <sub>2</sub> (?; n = 1/4)	Primary?		
			Albite	Fls: CH <sub>4</sub> , H <sub>2</sub> O	Primary?		
			Quartz	Fls: CH <sub>4</sub> (n = 1/2), H <sub>2</sub> O (n = 2/2)	Secondary?		
Kamuikotan (Hokkaido)	HKJ3 ( <i>jadeite</i> ; Fig. S22)	Jadeite	Fls: CH <sub>4</sub> , H <sub>2</sub> O (all, n = 2/2)	Secondary?	Cretaceous? (Hirajima, 2017)	Jadeite formation	
		Quartz	Fls: CH <sub>4</sub> (n = 1/2), H <sub>2</sub> O (n = 2/2)	Primary			
		Jadeite	Fls: CH <sub>4</sub> , H <sub>2</sub> O (all, n = 1/1)	Secondary?			
		Jadeite	Fls: CH <sub>4</sub> , H <sub>2</sub> O (all, n = 1/1)	Secondary?			
USA	New Idria	Cfn1 ( <i>jadeite</i> ; Fig. S28)	Jadeite	Fls: CH <sub>4</sub> , H <sub>2</sub> O (all, n = 6/6)	Secondary	Cretaceous?	Jadeite formation–retrogression (? Ma)
			Albite	Fls: CH <sub>4</sub> (n = 5/5), N <sub>2</sub> (n = 2/5), H <sub>2</sub> (n = 2/5), H <sub>2</sub> O (n = 5/5)	Primary		
			Jadeite	SIs: graphite	–		
Myanmar		N11 ( <i>jadeite</i> ; Fig. S29)	Analcime	Fls: CH <sub>4</sub> (n = 1/1)	Primary	146.5 ± 3.4 Ma Zrn U–Pb (Shi et al., 2008)	Jadeite formation
			Jadeite	Fls: CH <sub>4</sub> (n = 3/3), H <sub>2</sub> O (n = 2/3)	Pseudo-secondary?		
Kazakhstan		KZY-11 ( <i>jadeite</i> ; Fig. S26)	Jadeite	Fls: CH <sub>4</sub> , H <sub>2</sub> O (all, n = 3/3)	Secondary	ca. 450 Ma (Wen et al., 2023)	Jadeite formation–retrogression (? Ma)
Russia	Polar Urals	PUL ( <i>jadeite</i> ; Fig. S31)	Jadeite	Fls: CH <sub>4</sub> (n = 3/3), N <sub>2</sub> (n = 2/3), H <sub>2</sub> O (n = 3/3)	Secondary?	404 Ma Zrn U–Pb (Meng et al., 2011)	Jadeite formation–retrogression (? Ma)
	Chukotka	RSA1 ( <i>jadeite</i> ; Fig. S32)	Jadeite	Fls: CH <sub>4</sub> , H <sub>2</sub> O (all, n = 1/1)	Primary	Late Paleozoic	Jadeite formation
	West Sayan	SYN ( <i>jadeite</i> ; Fig. S30)	Jadeite	Fls: CH <sub>4</sub> (n = 3/3), H <sub>2</sub> O (n = 2/3)	Primary	Early Paleozoic?	Jadeite formation
Western Alps (Italy)	Lanzo Massif	1Bal17-4e1 ( <i>jadeite</i> ; Fig. S27)	Jadeite	Fls: CH <sub>4</sub> (n = 3/4), H <sub>2</sub> (n = 2/4), H <sub>2</sub> O (n = 4/4) SIs: graphite	Primary –	49.6 ± 1.0 Ma ( Piccoli et al., 2023)	Jadeite formation
			Garnet	Fls: CH <sub>4</sub> (n = 7/7), H <sub>2</sub> (n = 4/7) SIs: graphite	Primary –		

### 2.3. Modeling of C-O-H fluid speciation

Fig. 5 was constructed by modeling of C-O-H fluid speciation at graphite-saturated conditions using the Thermotopes-COH software

(Boutier et al., 2024a). Pressure–temperature (P–T) diagrams showing CH<sub>4</sub>/(CH<sub>4</sub> + CO<sub>2</sub>) ratios were constructed by considering fixed *f*O<sub>2</sub> values from –3 to +1 log units relative to the fayalite-magnetite-quartz (FMQ) buffer. The carbon activity was set to 1 to impose graphite-

saturated conditions. Water-maximum conditions (Fig. 5a) impose equal proportions of CH<sub>4</sub> and CO<sub>2</sub> for graphite-saturated fluids throughout the P–T space (Connolly and Cesare, 1993). The diagrams also report P–T conditions of a global collection of metamorphic rocks (shown as filled circles in Fig. 5) used by Brown and Johnson (2019) to derive evolving geothermal gradients through Earth's history. In Fig. 6b, for the same pressure–temperature couples (plotted from 1.2 Ga onwards), *f*O<sub>2</sub> values relative to the FMQ buffer resulting from Fig. 5 were plotted as a function of their age (filled circles corresponding to CH<sub>4</sub>/(CH<sub>4</sub> + CO<sub>2</sub>) ratios at between FMQ and FMQ-2 in Fig. 6b). Fig. 5 (gray field) also shows qualitative P–T constraints for the considered jadeitites (from Harlow et al., 2015). The results of our modeling are presented in the discussion (Sect. 4.2) to ensure fluent reading of this work, which would be hampered by presenting them earlier in the text. Output values of our thermodynamic calculations are in the supplementary material (Table S7).

### 3. Results

#### 3.1. Fluid inclusion data and microstructural relations

Jadeitites and their retrogression products are the result of fluid–rock interaction. The investigation of FIs in primary (e.g., jadeite) and retrogression (e.g., titanite and albite) minerals therefore provide direct information on the chemical composition of fluids circulating in the mantle wedge at varying depths, from jadeite formation at > 35 km depths to shallower crustal depths. Here, we provide data of analyzed FIs in jadeite (i.e., deeper fluids), and in titanite, pectolite, albite, analcime, garnet and apatite (i.e., shallower fluids). Our findings are summarized in Fig. 1 and in Table 1, with detailed results and representative spectra shown in the Supplementary material (Table S1, and Figs. S1–S17) and each studied sample (except for samples GT1, OSJ1002 and R5 selected for titanite dating, which are described in detail below) described in Supplement C (Figs. S19–S32). As detailed below, in three of the studied localities we document, for the first time, the presence of CH<sub>4</sub> in jadeitites: North of the Motagua Mélange in Guatemala, and at Chukotka and West Sayan in Russia. While CH<sub>4</sub> had been detected in fluid inclusions in jadeite in Osayama jadeitites (Tsujimori, 2017), we report its occurrence in secondary minerals (i.e., titanite and pectolite) in these rocks for the first time here. In addition, our study is the first documentation of not only CH<sub>4</sub>, but also H<sub>2</sub> and N<sub>2</sub> in Osayama albitites (i.e., in garnet, apatite). To our knowledge, the only jadeite locality where H<sub>2</sub> had been reported before is the Lanzo Massif, in the Western Alps (Giuntoli et al., 2024), while the other occurrences presented here are unprecedented. Our study is also the first to report CH<sub>4</sub>, H<sub>2</sub> and N<sub>2</sub> in an albite vein and analcime in a jadeite sample from New Idria. Finally, in the Polar Urals and North of the Motagua Mélange, we document for the first time the occurrence of N<sub>2</sub> in jadeitites.

In Japan, CH<sub>4</sub> is detected in jadeite-hosted primary and secondary FIs (Figs. S2–S5 and S7–S9) in samples OSJ1002, KYJ3-2, KYJ3-4, Sk3, HKJ2 and HKJ3, in agreement with previous work (Tsujimori and Harlow, 2017). Jadeite in sample KYJ3-2 also hosts graphite (Fig. S4b), indicating that the circulating reduced fluid that precipitated graphite was C-saturated. In addition, our investigations reveal that graphite and CH<sub>4</sub>(± H<sub>2</sub>)-bearing primary and secondary FIs are present in other rock-forming minerals like albite, quartz, apatite, and grossular garnet (samples R5, FMAB and HKJ3; respectively, Figs. S3, S6–S7), while N<sub>2</sub> is only present in primary FIs in jadeite (sample KYJ3-2; Fig. S4a). Our data from jadeitites from Myanmar (sample FI-3-MYAM; Fig. S10) and Kazakhstan (sample KZY-11; Fig. S11) confirm the presence of CH<sub>4</sub> and H<sub>2</sub>O in jadeite-hosted FIs, consistently with previous studies (Shi et al., 2005; Wen et al., 2023). In addition to graphite (Figs. S12b and S12d), jadeite and grossular garnet in one jadeite (sample 1Ba17-4e1) from the Lanzo Massif (western Alps, Italy) host CH<sub>4</sub> and H<sub>2</sub> (± H<sub>2</sub>O) in primary FIs (Figs. S12a and S12c), in agreement with Giuntoli et al. (2024). Secondary and primary FIs in jadeite in one jadeite from New Idria

(USA; sample Cfn1; Fig. S13) host CH<sub>4</sub> (+ H<sub>2</sub>O). In this sample, albite-hosted FIs also bear N<sub>2</sub> and H<sub>2</sub>. Analcime in another jadeite sample from the same locality (sample NI1; Fig. S14) hosts primary CH<sub>4</sub>-rich FIs, and jadeite in the same sample hosts graphite. Analcime is a lower-P–T mineral compared to jadeite, whose formation is controlled by the reaction jadeite + H<sub>2</sub>O = analcime. This is predicted to occur at pressures below 0.45–0.60 GPa for temperatures between 200 and 300 °C (e.g., Harlow, 1994; Harlow and Sorensen, 2005; Tsujimori and Harlow, 2012; Harlow et al., 2015), indicating that CH<sub>4</sub> circulation occurred at depths shallower than ca. 15–20 km. Our measurements reveal CH<sub>4</sub> in primary FIs in jadeite in jadeitites from the Russian localities of West Sayan (sample SYN; Fig. S15) and from Chukotka (sample RSA1; Fig. S16). In the Polar Urals (Russia), only CH<sub>4</sub> had been previously documented (Meng et al., 2011), while N<sub>2</sub> is also revealed by our analyses (sample PUL; Russia; Fig. S17).

Previously undocumented CH<sub>4</sub>-rich FIs are also found in one jadeite (sample GT1) from north of the Motagua Fault (North Motagua Mélange, Guatemala), which represents the boundary between the North American and Caribbean plates (Harlow et al., 2016). Sample GT1 (Fig. 2a) is made of jadeite, locally replaced by albite, and it contains minor titanite and zircon. Jadeite and titanite include graphite (Fig. S1b and S1d), and they host, respectively, possibly primary and certainly secondary CH<sub>4</sub>–H<sub>2</sub>O ± N<sub>2</sub>-rich FIs (Fig. 1; Fig. S1a and S1c). This represents the first documentation of both CH<sub>4</sub> and N<sub>2</sub> in jadeitites from the North Motagua Mélange in Guatemala. Graphite is trapped during jadeite growth, and CH<sub>4</sub>-bearing fluids are trapped during or after jadeite and titanite growth in sample GT1 (Fig. 1). Since titanite formed after jadeite (Tsujimori and Harlow, 2012), this indicates protracted circulation of C-saturated fluids along the Guatemalan plate boundary, persisting between the time of jadeite formation (95–98 Ma; zircon U–Pb; Yui et al., 2010; see Sect. 4.1) at > 1 GPa (Harlow et al., 2015) and titanite crystallization. Notably, circulation of these fluids ended before jadeite retrogression to albite, as suggested by the lack of graphite and CH<sub>4</sub>-bearing FIs in albite.

Jadeite OSJ1002 and albitite R5 are from the Osayama serpentinite mélange in Japan (Tsujimori and Itaya, 1999; Tsujimori et al., 2005). In jadeite OSJ1002, jadeite and rutile precipitated together early, and pectolite and titanite are later phases (Tsujimori et al., 2005; Tsujimori and Harlow, 2012). The presence of two titanite generations (respectively, titanite1 and titanite2 hereafter) in this sample is suggested by the color of the crystals and on the presence vs. lack of inclusions: titanite1 grows on rutile, is brown in color and free of FIs, it includes jadeite grains, and it is overgrown by titanite2 (Fig. 2b). Titanite2 is colorless to pale brown, and it hosts solid inclusions. In sample OSJ1002, graphite is included in jadeite and titanite2 (Fig. 1; Fig. S2b–c), implying circulation of C-saturated fluids between jadeite precipitation and during titanite recrystallization. Secondary FIs (possibly primary FIs as well) are only observed in jadeite and pectolite, containing CH<sub>4</sub> (Fig. 1; Fig. S2a and S2d) in agreement with Tsujimori and Harlow (2017). Altogether, secondary FIs in jadeite and pectolite, and graphite inclusions in jadeite and titanite2 indicate that C–H(–O) fluids percolated in the Japanese mantle wedge at conditions of jadeite stability, as well as during and after jadeite retrogression during exhumation. This is supported by graphite and FIs in albitite R5, which is considered as the retrogressed equivalent of jadeite OSJ1002. Albitite R5 (Fig. 2c) is made of albite, rutile, titanite, grossular garnet (see Tsujimori and Harlow, 2012), apatite and relict diopside. Here, graphite is included in titanite and albite (Fig. 2; Fig. S3c and S3e). Secondary FIs in titanite contain CH<sub>4</sub>, H<sub>2</sub>, and possibly CO<sub>2</sub> and NH<sub>4</sub> (i.e., the peaks of CO<sub>2</sub> and NH<sub>4</sub> are not clearly identified; Fig. S3a–b), those hosted by grossular garnet CH<sub>4</sub>, N<sub>2</sub>, and H<sub>2</sub>O (Fig. S3d), and those hosted by apatite CH<sub>4</sub> and H<sub>2</sub> (Fig. S3f). To our knowledge, these chemical species had not been reported before in such metasomatic rocks. No FIs are observed in albite, indicating that titanite formed before albite during exhumation, although the time span between titanite and albite crystallization cannot be constrained.

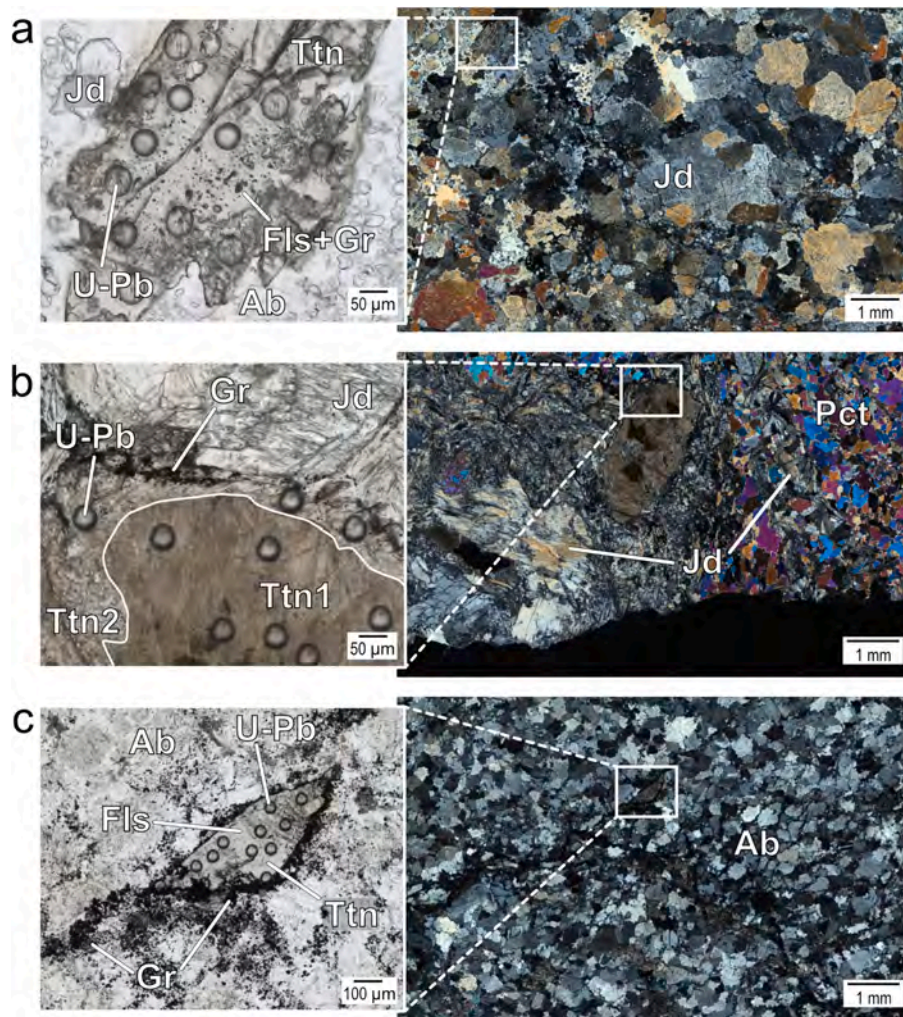


**Fig. 2.** Transmitted-light photomicrographs of the samples selected for titanite geochronology. (a) GT1 and (b) OSJ1002 jadeites, and (c) R5 albite. Ab = albite; Fls = fluid inclusions; Gr = graphite; Jd = jadeite; Pct = pectolite; Ttn = titanite; U-Pb = craters from U-Pb dating. Photomicrographs on the left-hand side are in plane-polarized light, while those on the right-hand side are in cross-polarized light. Acquired using the ZEISS ZEN core software (version 3.6).

Most of the identified FI host minerals are free of or poor in redox-sensitive elements such as Fe, indicating that the presence of reduced fluid species such as  $H_2$  and  $CH_4$  does not result from post-entrapment interactions of the fluid with the host minerals. The  $CH_4$ -dominated composition of FIs in the studied rocks clearly reflects the reduced nature of the trapped metamorphic fluids, although an increase in  $CH_4/CO_2$  ratio is expected for graphite-saturated FIs during cooling (Cesare, 1995). The presence of graphite inclusions in jadeite (Guatemala, Osayama, Itoigawa–Omi, Lanzo Massif), as well as in secondary titanite (Guatemala and Osayama), pectolite (Osayama) and albite (Osayama; Fig. 2), implies that C-rich fluids circulated along higher-P jadeites and lower-P albitites during multiple events of fluid percolation at varying depths and across the entire Phanerozoic eon. This is corroborated by  $CH_4 \pm N_2$ -bearing FIs in high-P jadeite in plate-interface metasomatic rocks at several convergent plate boundaries – i.e., Guatemala, Osayama, Itoigawa, Kazakhstan, New Idria, Myanmar, Polar Urals, West Sayan, and the Lanzo massif (Western Italian Alps). The protracted circulation of energy sources at shallower depths is demonstrated by their presence in lower-P minerals (e.g., albite, analcime) in similar rocks from New Idria and Japan.

### 3.2. Zircon and titanite U–Pb geochronology

U–Pb geochronology by LA-ICP-MS was used to determine the timing

of crystallization of titanite in samples GT1, OSJ1002, and R5, and of zircon OSJ-T05 from Osayama, already described in Tsujimori et al. (2005). Titanite in Guatemalan sample GT1 gave an age of  $71.8 \pm 4.0$  Ma (mean square of weighted deviates, MSWD = 1.4; number of analyses,  $n = 27$ ) with an initial  $^{207}Pb/^{206}Pb$  ratio of  $0.841 \pm 0.007$  (Fig. 3a).

As for the Japanese samples, zircon U–Pb geochronology returned an age of  $523.6 \pm 3.5$  Ma (MSWD = 0.76;  $n = 26$ ), with no calculated initial  $^{207}Pb/^{206}Pb$  ratio (Fig. 3b). Titanite in sample OSJ1002 (Fig. 3c) returned an age of  $464.8 \pm 20.3$  Ma (MSWD = 0.95,  $n = 44$ ) with an initial  $^{207}Pb/^{206}Pb$  value of  $0.861 \pm 0.006$ . No resolvable differences in age or initial  $^{207}Pb/^{206}Pb$  ratios are revealed by Tera–Wasserburg regressions of titanite1 ( $475.3 \pm 32.0$  Ma and initial  $^{207}Pb/^{206}Pb$  ratio of  $0.863 \pm 0.008$ ; MSWD = 0.95;  $n = 33$ ) and titanite2 ( $458.1 \pm 28.0$  Ma and initial  $^{207}Pb/^{206}Pb$  ratio of  $0.860 \pm 0.014$ ; MSWD = 1.1;  $n = 11$ ) plotted separately. The MSWD value of 0.95 of a Tera–Wasserburg regression given by U–Pb isotope data of titanite1 and titanite2 combined confirms that the two titanite generations are coeval within uncertainty. Titanite in sample R5 yielded an age of  $466.1 \pm 4.4$  Ma (MSWD = 1.3;  $n = 28$ ) with an initial  $^{207}Pb/^{206}Pb$  ratio of  $0.864 \pm 0.020$  (Fig. 3d). One way to test if titanite in samples OSJ1002 and R5 formed during the same retrogression event is to plot their U–Pb isotope datasets in one Tera–Wasserburg diagram, and to assess if the MSWD value is close to 1. In one Tera–Wasserburg plot, titanite from samples OSJ1002

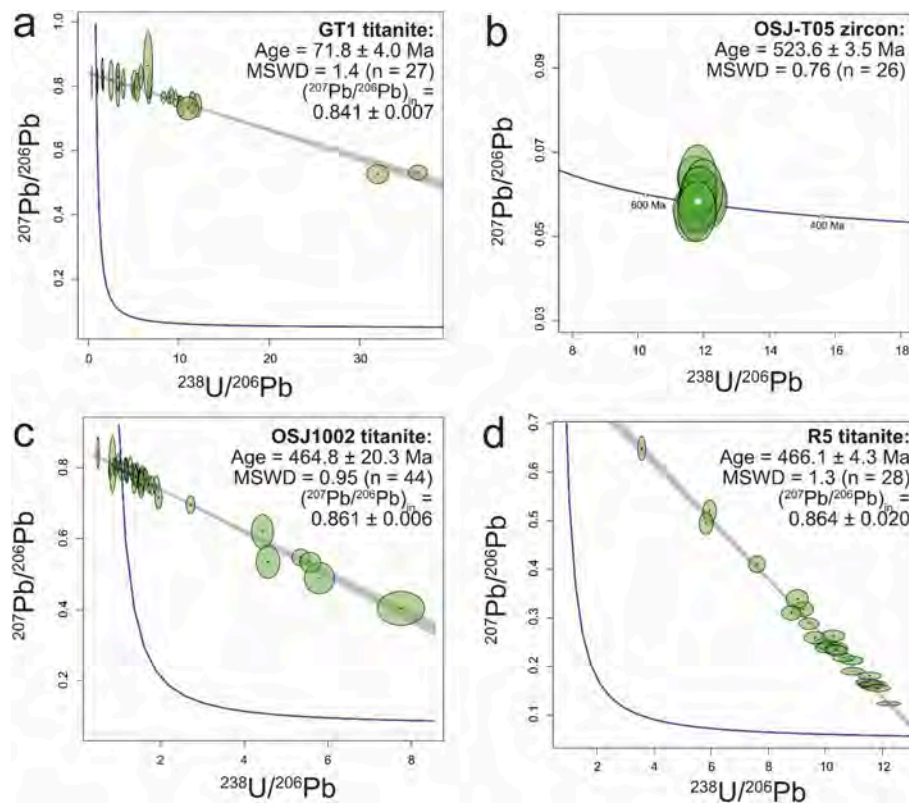


**Fig. 3.** Tera–Wasserburg diagrams of (a) titanite in jadeitite GT1, (b) OSJ-T05 zircon, (c) titanite in jadeitite OSJ1002, and (d) titanite in albitite R5. Age uncertainties are given at 95 % confidence level and error ellipses are  $2\sigma$ . Plotted using IsoplotR (Vermeesch, 2018).

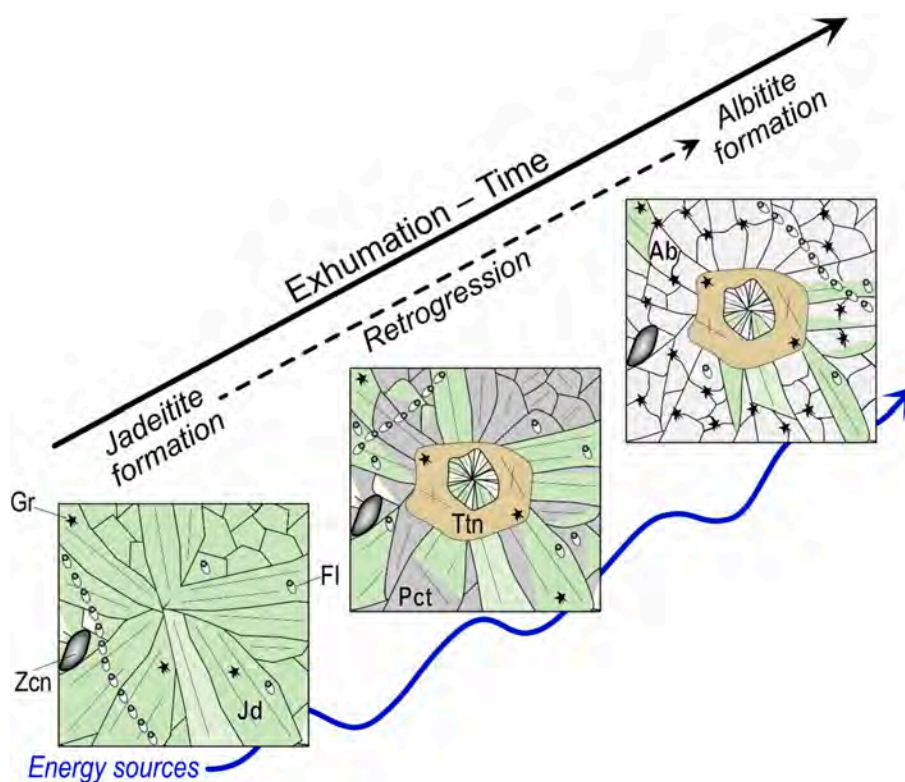


**Fig. 4.** Conceptual sketch of microstructures produced during jadeitite formation and retrogression, with dateable minerals (i.e., zircon and titanite) crystallizing at different stages/depths, thus dating different events. Ab = albitite; FI = fluid inclusion; Jd = jadeite; Pct = pectolite; Ttn = titanite; Zcn = zircon. All envisaged in plane-polarized light. Not to scale.

and R5 gave an age of  $465.5 \pm 3.0$  Ma with an MSWD value of 1.0 ( $n = 72$ ). This indicates that only one titanite generation is resolvable at the available analytical precision, hinting that retrogression of sample OSJ1002 and of the protolith of sample R5 were related to the same exhumation event.

## 4. Discussion

### 4.1. Protracted $CH_4$ – $H_2$ circulation towards the biotic fringe

Dating jadeitite crystallization is a challenging task (see Tsujimori and Harlow, 2012; Harlow et al., 2015). While some minerals like titanite, albite, and analcime are accepted as secondary phases forming during recrystallization or cooling/retrogression of jadeitites (Tsujimori and Harlow, 2012), zircon has been variably interpreted as either primary – thus dating the formation of jadeitites – or inherited – thus yielding ages that are older than those of jadeitite formation (Fu et al., 2010; Tsujimori and Harlow, 2012; Harlow et al., 2015). The following discussion is based on the thorough review of existing geochronological and petrographic data by Tsujimori and Harlow (2012). The use of our newly obtained data and those compiled in the cited literature allows us to evaluate and discuss the time lapses in which C-saturated fluids precipitated graphite as solid inclusions by considering the proposed timing of jadeitite formation – and graphite inclusions therein – as the upper temporal limit, and that of titanite formation as the lower one (Fig. 4). If secondary FIs are included in secondary minerals (among which titanite), then the time lapses over which C-saturated fluids circulated may extend beyond their crystallization (Fig. 4) depending on whether these secondary FIs were formed by fluid influx after titanite formation rather than by decrepitation of primary FIs during deformation.

Because titanite is interpreted as a secondary mineral phase in jadeitites (Tsujimori and Harlow, 2012), the titanite age of  $71.8 \pm 4.0$  Ma obtained in jadeitite GT1 (Fig. 3a) pinpoints the timing of jadeitite retrogression. Titanite is hence ca. 20–30 Myr younger than jadeitite formation, which was dated at 98–95 Ma by U–Pb geochronology of zircon that was interpreted to have crystallized during jadeitite formation (Yui et al., 2010). Therefore, the presence of graphite as a solid inclusion in primary jadeite and secondary titanite, and the presence of secondary  $CH_4$ -bearing FIs in titanite in sample GT1 (Fig. 2) testifies circulation – episodic or continuous – of C-saturated fluids potentially for at least ca. 20–30 Myr in the Guatemalan mantle wedge.

As noted in the literature (Tsujimori et al., 2005), zircon grains in jadeitites from Osayama include rutile and jadeite, and they are therefore interpreted as dating the timing of jadeitite formation, which occurred  $523.6 \pm 3.5$  Ma according to our data (Fig. 3b). Titanite in samples OSJ1002 and R5 indicates that retrogression of jadeitites occurred  $465.5 \pm 3.0$  Ma, which is ca. 60 Myr after jadeitite formation. Given the presence of graphite in jadeite and titanite, circulation of C-saturated fluids in the Japanese mantle wedge began during jadeitite formation and continued at least until titanite formation, namely for ca. 60 Myr. The presence of primary (in garnet) and secondary (in apatite)  $CH_4$ -,  $H_2$ -, and  $H_2O$ -bearing FIs in other secondary minerals (Tables 1 and S1), indicates that the circulation of deep energy sources in the Japanese mantle wedge lasted up to shallower depths when primary and secondary FIs formed in lower-P minerals.

We cannot obtain our own geochronological constraints on timing and duration of circulation of energy sources in the other jadeitite locations due to the lack of dateable  $CH_4$ -hosting minerals. However, the timing of jadeitite formation and retrogression is available from the literature for several of these localities (Table 1) and can be inferred from microstructural relations between FIs and host minerals (Fig. 4). In Itoigawa–Omi, jadeitite formation is dated at ca. 536–505 Ma linking zircon U–Pb ages of  $519 \pm 17$  Ma and  $512 \pm 7$  Ma to the precipitation of jadeitite (Kunugiza and Goto, 2010; Tsujimori and Harlow, 2012), and retrogression at ca. 350–320 Ma (Tsujimori and Harlow, 2012). This

indicates that circulation of deep energy sources lasted for up to ca. 200 Myr between the formation of primary  $CH_4$ -bearing FIs in primary jadeitite and in secondary albite (Table 1). Methane circulation in the Lanzo Massif was dated at  $49.6 \pm 1.0$  Ma by perovskite U–Pb geochronology (Piccoli et al., 2023), but no temporal constraints exist for any retrogression. In Myanmar, the timing of jadeitite formation, hence entrapment of pseudosecondary  $CH_4$ -bearing FIs, is dated at  $146.5 \pm 3.4$  Ma (Shi et al., 2008), and that of retrogression at 147–122 Ma (Tsujimori and Harlow, 2012). For the Polar Urals, only a U–Pb age of zircon of  $404 \pm 7$  Ma – interpreted as dating the formation of jadeitite – is available from Meng et al. (2011), indicating that migration of  $CH_4 \pm N_2$  occurred at this time either in the jadeitite stability field or at unconstrained similar or shallower depths based on the presence of secondary  $CH_4$ -bearing FIs in jadeite (Table 1). The timing of jadeitite formation in New Idria and in West Sayan is not ascertained, but it may have occurred in the Cretaceous and in the Early Paleozoic, respectively (Tsujimori and Harlow, 2012). Thus,  $CH_4$  circulation in New Idria must have occurred either in the Cretaceous during jadeitite formation or at shallower depths, as indicated by primary FIs in albite and analcime, and secondary  $CH_4$ -bearing FIs in jadeite, while in West Sayan primary  $CH_4$ -bearing FIs in jadeite indicate  $CH_4$  circulation in the Early Paleozoic (Table 1). Finally, the timing of jadeitite formation in Kazakhstan is estimated at ca. 450 Ma (Wen et al., 2023). Therefore,  $CH_4$  circulation occurred at this time or shortly after, based on the presence of secondary  $CH_4$ -bearing FIs in jadeite (Table 1).

According to literature, C–H–N–O–P–S species produced by deep geological processes sustain subsurface microbial life at convergent margins (e.g., Mottl et al., 2003; Ohara et al., 2012; Plümper et al., 2017; Barry et al., 2019; Fullerton et al., 2021), and the plate interface is a viable fluid conduit for such deep fluids (e.g., Marschall and Schumacher, 2012; Bebout and Penniston-Dorland, 2016; Angiboust et al., 2021b,a). In order to sustain a subsurface biosphere at convergent margins, the delivery of deeply sourced energy sources above the biotic fringe must be protracted over time. Jadeitites are often interpreted as resulting from infiltration of the mantle by sediment-derived serpentinizing fluids (Shi et al., 2005; Harlow et al., 2015; Chen et al., 2023). The fact that these rocks form along the plate interface and are progressively exhumed in subduction complexes implies that they are flushed by fluids released by dehydration of the subducting slab, which jadeitites have also been proven to channelize (Tsujimori and Harlow, 2012; Harlow et al., 2015; Angiboust et al., 2021b,a). The evidence recorded by solid and fluid inclusions in plate-interface metasomatic rocks (Table 1) indicates that building block elements and energy sources for microbial life percolate along plate-interface rocks from their formation at high P to their retrogression at lower-P conditions (Fig. 6a), potentially for tens/hundreds of millions of years. The presence of  $CH_4$  and  $H_2$  in lower-P minerals (particularly albite and analcime, as retrogression mineral phases in jadeitites) demonstrates circulation of energy sources at shallower depths as well (Fig. 6a; from depths as shallow as ca. 20–15 km based on the occurrence of analcime). Hence, such fluid fluxes may have reached the biotic fringe for a protracted period of time, thus feeding subsurface microbial communities similarly to several present-day case studies (Mottl et al., 2003; Ohara et al., 2012; Barry et al., 2019, 2022; Fullerton et al., 2021; Rogers et al., 2023; Upin et al., 2023).

### 4.2. Viability, origins, and amounts of graphite-saturated reduced fluids in plate-interface rocks

Although our fluid inclusion data already show that trapped fluids were dominantly reduced (Table 1), hence that the dominant carbon species was  $CH_4$  rather than  $CO_2$ , the present section provides further support in this respect by combining thermodynamic data with varying conditions (e.g., P, T, oxygen fugacity ( $fO_2$ ), carbon input, and geological time) possible in subduction as slab-derived fluids are released and channelized through jadeitites during their formation and retrogression.

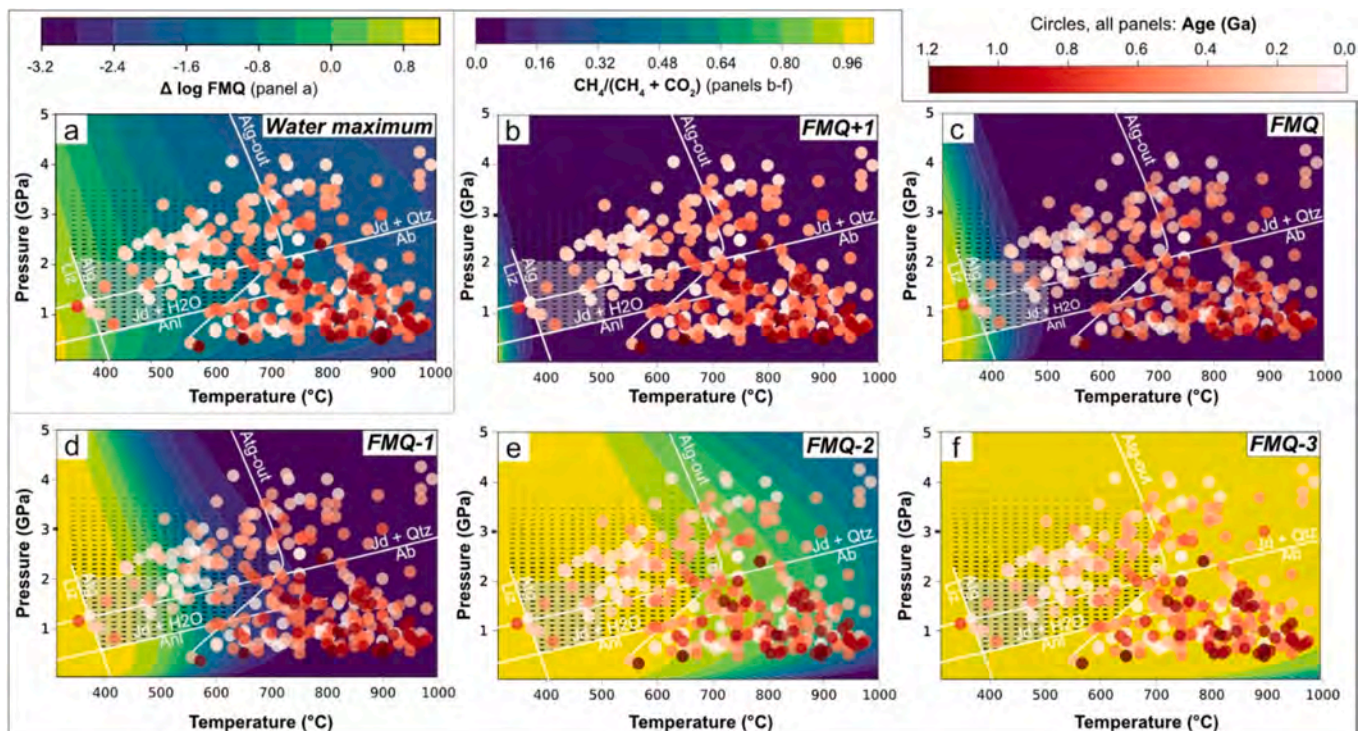


**Fig. 5.** (a) Redox conditions (expressed as  $\Delta \log \text{FMQ}$ ) of graphite-saturated fluids at the water maximum (see Connolly and Cesare, 1993) expected at the P–T conditions of jadeite formation. (b–f) P–T diagrams at varying redox conditions – expressed relative to the fayalite-magnetite-quartz (FMQ) buffer – from FMQ+1 to FMQ-3 for graphite-saturated C–O–H fluids, showing how higher P conditions favor the stability of reduced carbon species (i.e.,  $\text{CH}_4$ ) over that of oxidized ones (i.e.,  $\text{CO}_2$ ). The filled circles are metamorphic rocks of different ages (different red shades) from Brown and Johnson (2019), whose peak P–T conditions were used to calculate corresponding  $\text{CH}_4/(\text{CH}_4 + \text{CO}_2)$  ratios. The dashed pattern is the superposition of preserved high-pressure rocks (from Brown and Johnson, 2019) and the stability field of jadeitites from Harlow et al. (2015). The gray field indicates the stability field of jadeitites proposed by Harlow et al. (2015). Plotted using the Thermotopes-COH software (Boutier et al., 2024b).

The depths from which metamorphic fluids can rise is dependent upon slab dip and geothermal gradients, and by the formation of preferential fluid pathways such as plate-interface discontinuities (e.g., Wilson et al., 2014) or lithologies such as the studied jadeitites (Harlow and Sorensen, 2005; Harlow et al., 2015; Angiboust et al., 2021b,a). Overall, metamorphic regimes have varied progressively towards lower temperature/higher pressure gradients over geological time (e.g., Gerya, 2014; Brown and Johnson, 2019; Dewey et al., 2021; Holder et al., 2019). Cooling thermal gradients over geological time have favored the transfer of slab-bound water – and thereby the source region of metamorphic fluids returning to the Earth’s surface – to greater depths (van Keken et al., 2011), and has necessarily impacted the nature of metamorphic fluids and their redox state as discussed in the following.

The widespread presence of graphite in jadeitites and albitites (Figs. 2, S1b, S1d, S2b–c, S3c, S3e, S4b, S12b, S12d and S14a; Tables 1 and S1) indicates that fluids migrating along these domains in subduction settings are remarkably graphite-saturated. Graphite-saturated fluids may form either through the evolution of formerly graphite-undersaturated fluids – for example, during rock hydration reactions such as serpentinization – or from the infiltration of aqueous fluids generated from, or equilibrated with, graphite-bearing rocks (Holloway, 1984; Duke and Rumble, 1986). In our case, this second scenario is supported by the only known carbon isotopic composition of  $\text{CH}_4$  from jadeite-hosted FIs in Myanmar jadeitites ( $\delta^{13}\text{C}\text{-CH}_4 = -30$  to  $-26$  ‰; Shi et al., 2005), which suggests the contribution of a biogenic source of organic matter such as subducted graphitic schists. The involvement of sediment-derived fluids in the formation of jadeitites is also supported by Fe isotopes in samples from Myanmar (Chen et al., 2023), and by Li and O isotopes in samples from New Idria (Sorensen et al., 2006; Takahashi et al., 2018).

The early metamorphic path of organic matter-rich rocks is expected

to release  $\text{CH}_4$ -rich fluids during carbonization and high-temperature thermogenic processes (e.g., Manguet et al., 2021). At higher T, graphitic carbon resulting from metamorphism of organic matter is expected to impart a strong buffering potential to aqueous fluids. It has been proposed that the redox state of fluids released during prograde dehydration of graphite-bearing pelitic schists maintains H:O ratios equal to 2:1 – the so-called water maximum for graphite-saturated C–O–H fluids (Connolly and Cesare, 1993). At water-maximum conditions (Fig. 5a), graphite-saturated C–O–H fluids contain equal proportions of  $\text{CO}_2$  and  $\text{CH}_4$ , with  $f\text{O}_2$  conditions changing with P and T. This condition would imply that prograde metamorphism of graphitic schists releases a substantial amount of  $\text{CH}_4$ , comparable to that of  $\text{CO}_2$  produced by the same process. Because the persistence of water-maximum conditions cannot be verified – for example, for more oxidized or reduced systems buffered by other rock-forming minerals or in the case of infiltration of external fluids (Connolly and Cesare, 1993; Huff and Nabelek, 2007) – we calculated  $\text{CH}_4/(\text{CH}_4 + \text{CO}_2)$  ratios in graphite-saturated fluids for different  $f\text{O}_2$  conditions spanning from reduced (FMQ-3) to oxidized (FMQ+1) conditions for the same P–T range (Fig. 5b–f). The range of redox conditions of  $\text{FMQ-2} \leq f\text{O}_2 \leq \text{FMQ}$  is consistent with estimates from natural graphite-bearing metasedimentary rocks and thermodynamic modeling (Huff and Nabelek, 2007; Padrón-Navarta et al., 2023), and they also overlap with redox conditions predicted for subduction zone serpentinization (Vitale Brovarone et al., 2020). The  $\text{CH}_4/(\text{CH}_4 + \text{CO}_2)$  ratio of each of these P–T couples reported in Fig. 5b–f and 6b was calculated for each  $f\text{O}_2$  value. According to our modeling, while at conditions of FMQ-2 or lower graphite-saturated fluids are all  $\text{CH}_4$ -dominated regardless of thermal gradient (i.e., different P–T conditions shown as solid circles in Fig. 5e–6b), higher  $\text{CH}_4/(\text{CH}_4 + \text{CO}_2)$  mole ratios are favored by P–T conditions typical of cooler thermal regimes at FMQ-1 (Fig. 5d) and FMQ (Fig. 5c). Notably, such conditions are more

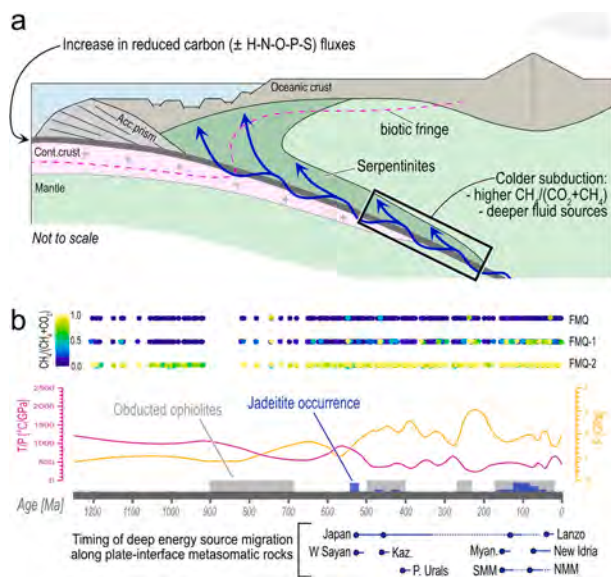


**Fig. 6.** (a) Schematic of a Phanerozoic subduction zone and redistribution of deep energy sources from deeper to shallower levels. Acc. = accretionary; Cont. = continental; (redrawn from Vitale Brovarone et al., 2020). (b) Timeline of occurrence of dated plate-interface metasomatic rocks (our data combined with Tsujimori and Harlow, 2012), and comparison with the variation of subduction thermal gradients (represented as the purple T/P curve redrawn from Huang et al. (2023) and based on the data of Brown and Johnson (2019)), maximum pressures recorded by metamorphic rocks (represented as the yellow P curve redrawn from Huang et al. (2023) and based on the data of Brown and Johnson (2019)), the occurrence of obducted suprasubduction ophiolites (from Stern et al., 2013; Dilek, 2003), and the  $\text{CH}_4/(\text{CH}_4 + \text{CO}_2)$  ratios calculated at FMQ to FMQ-2 using the P-T conditions of the compilation of metamorphic rocks from Brown and Johnson (2019). Kaz. = Kazakhstan; MYAN = Myanmar; NMM = North Motagua Mélange; P. Urals = Polar Urals; SMM = South Motagua Mélange; W Sayan = West Sayan. Dashed blue lines indicate uncertainties in the duration of fluid circulation or in the age or rock formation.

frequently encountered in Phanerozoic metamorphic terranes (Figs. 5 and 6b). More oxidized (FMQ+1; Fig. 5b) conditions show negligible variations between hot and cold subduction thermal regimes.

Overall, our calculations show that cooler subduction regimes, and P-T conditions overlapping with jadeite formation (Fig. 5), stabilize reduced carbon species (i.e.,  $\text{CH}_4$ ) relative to oxidized ones (i.e.,  $\text{CO}_2$ ). However, because the solubility of graphite increases with increasing T and decreases with higher P (Connolly and Cesare, 1993), under cooler plate-tectonic regimes – hence, slab dehydration occurring at lower T and higher P – the total amount of carbon (including absolute amounts of  $\text{CH}_4$ ) dissolved in a graphite-saturated fluid is lower than under warmer plate-tectonic regimes. This effect may have been partially counterbalanced via secular or episodic increases in total reduced carbon being subducted in sediments. In fact, a gradual increase in total carbon contents from the Phanerozoic is documented in the preserved record of black shales (Sperling and Stockey, 2018), and C isotope data are consistent with an increase in subducted carbon in this eon (Giuliani et al., 2022). Earlier in Earth's history, between 2.0 and 1.7 Ga, the Paleoproterozoic Shunga event was characterized by maxima in black shale deposition, with less prominent peaks in the late Neoproterozoic between 800 and 600 Ma (Condie et al., 2001; and references therein). However, because of preservation bias due to the formation of the Great Unconformity at the Neoproterozoic–Phanerozoic boundary, the extent of the increase in volumes of subducted carbon is not clear. The present data and earlier work cannot demonstrate or rule out that a large enough increase in subducted C counterbalanced the smaller amounts of total dissolved carbon in slab-derived fluids. Nevertheless, our thermodynamic calculations demonstrate that such fluids were dominantly reduced and dominated by  $\text{CH}_4$ . Experimental work (Shock, 1990)

indicates that  $\text{CH}_4$  respiciation during cooling can be kinetically inhibited, favoring its metastable preservation in uprising fluids and potentially overstepping local redox heterogeneities. Previous estimates (Piccoli et al., 2021) indicate the channelized fluid fluxes in subduction zones (e.g., along the plate interface) may be very high (up to  $10^5$ – $10^6$   $\text{m}^3 \text{m}^{-2}$ ). This, together with the reduced fluid speciation identified in our global collection of plate-interface metasomatic rocks, suggests that large amounts of molecules such as  $\text{CH}_4$  and  $\text{H}_2$  can be delivered to the biotic fringe (Fig. 6a).

### 4.3. Cooler metamorphic gradients and deep biogeochemical cycles

Cold-subduction metamorphism is allegedly typical of the Neoproterozoic/Phanerozoic eons (e.g., Gerya, 2014; Brown and Johnson, 2019; Dewey et al., 2021). Although it is outside the scope of this work to settle ongoing debates regarding subduction styles over geological time, two points should be mentioned here. Firstly, the transition into modern-style plate tectonics was gradual (Fischer and Gerya, 2016; Holder et al., 2019). The occurrence of Archean eclogites argues that cold-subduction regimes similar to present-day ones may have occurred in pre-Cambrian times (Perchuk et al., 2019). Secondly, changes in subduction regimes also occur during the evolution of a single subduction zone, with warmer gradients during the early stages and cooler ones as subduction progresses (Holt and Condit, 2021). Therefore, while the present discussion focuses on the Phanerozoic eon, it cannot be excluded that similar considerations may apply to colder subduction zones outside the Phanerozoic eon. One limitation to the present discussion is that the emergence of large carbonate shelves in the Mesozoic and their subduction (Müller et al., 2022; Walton and Shorttle, 2024) implies a change in the redox state of carbon fed to subduction zones.

Important changes occurring over geological time favorably overlapped in the Neoproterozoic/Phanerozoic (Fig. 6b): decreasing thermal subduction regimes over geological time (e.g., Brown and Johnson, 2019) (represented by the purple T/P curve in Fig. 6b) allow rocks to be subducted to greater depths and lower temperatures than before (Brown and Johnson, 2019) (depicted as the yellow P curve in Fig. 6b); the redox state of slab-derived fluids was dominantly reduced (depicted as filled circles at FMQ-2 to FMQ in Fig. 6b); and fluxes of such fluids from the slab interface towards the biotic fringe were protracted in time (timeline in Fig. 6b). As a consequence of the Cambrian explosion, variably larger amounts of organic, reduced carbon – including not only C and H, but also other life-building block elements such as N, S and P (Ingall and Cappellen, 1990; Zerkle, 2018; Walton et al., 2023) – may have been fed to subduction zones (Husson and Peters, 2017; Walton et al., 2023). Carbon, H, N, S, and P are also key ligands for metals at varying Eh-pH conditions and they mediate transport and deposition of metals in ore deposits (e.g., Seward et al., 2014). Carbon isotope data of  $\text{CH}_4$  in FIs in jadeitites from Myanmar indicate an organic source of C in these Jurassic/Cretaceous samples (Shi et al., 2005). This, along with Fe isotope evidence (Chen et al., 2023), supports the involvement of subducted sediments rich in organic matter in the production and cycling of  $\text{CH}_4$  detected in plate-interface metasomatic rocks. Reduced redox states of slab-derived fluids favor transport of transition metals in the lithosphere (e.g., Bourg and Loch, 1995). This has far-reaching implications, because life uses first- and second-row transition metals as key centers in redox proteins responsible for the utilization of reduced compounds such as  $\text{H}_2$  and  $\text{CH}_4$  as electron donors in energy-conserving microbial reactions (e.g., Hay Mele et al., 2023; Giovannelli, 2023). Within these proteins, which are essential for microbial life, the metals are key co-factors mediating electron transfer and cycling. The diversity of substrates used by microbial life as energy sources (e.g.,  $\text{H}_2$  and  $\text{CH}_4$ ) is directly linked to the diversity and availability of diverse metals, since different compounds require dedicated proteins containing specific metals (e.g., Giovannelli, 2023). For example,  $\text{H}_2$ -utilizing proteins are known to use either a NiFe, FeFe or Fe only metal centers, while  $\text{CH}_4$ -oxidizing proteins require either Fe, Cu, or Ni depending on the specific

metabolic pathway (e.g., Hay Mele et al., 2023; Greening et al., 2024). The interplay between redistribution of C, H, N, O, P and S from the surface to subduction and from the plate interface to shallower depths, and the favorable transport of critical biological metals towards the biotic fringe under reduced conditions (e.g., Bourg and Loch, 1995) may have promoted the diversification of metabolic pathways and the proliferation of metabolically diverse microbial communities in the subsurface of cold subduction settings (e.g., Rempfert et al., 2017; Moore et al., 2017; Lima-Zaloumis et al., 2022; Giovannelli, 2023; Greening et al., 2024).

#### 4.4. Obducted ophiolites as evidence for migration of energy sources through time?

Serpentinization of mantle rocks – and consequent production of CH<sub>4</sub> and H<sub>2</sub> – has been proposed to be a key mechanism in the origin and sustainment of microbial life (Russell et al., 2010; Lima-Zaloumis et al., 2022). Active utilization and/or cycling of CH<sub>4</sub> and H<sub>2</sub> have been documented in suprasubduction ophiolites at different convergent margins: the Tablelands Ophiolite (Newfoundland, Canada; Brazelton et al., 2012), the Zambales Ophiolite (Philippines; Woycheese et al., 2015), the Tekirova Ophiolite (Turkey; Neubeck et al., 2017; Schwarzenbach et al., 2021; Etiope, 2023) and the Semail Ophiolite (Oman; Leong et al., 2023). Suprasubduction ophiolites are targeted as a key environment to search for evidence for microbial activity being affected by CH<sub>4</sub> and H<sub>2</sub> formed during active serpentinization (e.g., Brazelton et al., 2012; Rempfert et al., 2017; Neubeck et al., 2017; Trutschel et al., 2023). For their structural position and temporal distribution, obducted suprasubduction ophiolites are also the ideal target for the investigation of ancient subsurface microbial activity benefiting from the rise of deep energy sources along paleo-plate interfaces: Fig. 6b shows a fair match between the temporal distribution of jadeitites and Phanerozoic obducted suprasubduction ophiolites. Although jadeite localities do not provide access to the corresponding obducted suprasubduction ophiolites, this temporal match supports that the latter may very well record the transfer of deep metamorphic fluids carrying CH<sub>4</sub>-H<sub>2</sub> identified in jadeitites and albitites worldwide to habitable conditions in the subsurface biosphere. Flushing of C-rich plate-interface fluids is demonstrated at the base of obducted ophiolites, as recorded by the migration of CO<sub>2</sub>-rich fluids (de Obeso et al., 2021). In addition to this, the identification of solid reduced carbon compounds at the base of ophiolitic massifs (Kelemen et al., 2022) may represent fossil evidence for the migration of deep reduced fluids acting as energy sources in the subsurface biosphere of forearcs associated with cold subduction. In light of the present data and of their match with biogeodynamic events (Fig. 6b), obducted suprasubduction ophiolites may bear evidence for the combination of key factors contributing to diversification and flourish of subsurface microbial activity at convergent margins in a cold subduction regime.

## 5. Conclusions and outlook

We have presented chemical and geochronological data, showing that plate-interface metasomatic rocks record protracted, possibly episodic, fluxes of reduced chemical species like CH<sub>4</sub> and H<sub>2</sub> during their formation and exhumation through the mantle wedge. This implies that they have the potential to transfer such deeply tapped energy sources to shallower levels where they can feed subsurface microbial life in forearc regions, as documented in present-day case studies. Our thermodynamic modeling confirms that the stability of reduced chemical species is favored by cooler subduction geodynamics, which – based on the preserved geological record – have been suggested to be typical of the Neoproterozoic/Phanerozoic eons. While the latter point is debated and the discussion of our study may extend to cold subduction regimes in the pre-Cambrian, the Neoproterozoic/Phanerozoic geological record shows overlap among stability of reduced chemical species, variably

larger input of organic carbon in subduction, and colder geodynamics. Our work offers an explanation to the proliferation of subsurface microbial life in forearc regions in the Phanerozoic eon. However, it cannot be excluded that such conditions overlapped in pre-Cambrian times as well under similarly cool geothermal gradients, hence enhancing the applicability of our work.

## Data availability

Measured U–Pb isotope data (Tables S4–S6) and output values of thermodynamic modeling (Table S7) are available through Zenodo at <https://zenodo.org/doi/10.5281/zenodo.12680604>.

## CRediT authorship contribution statement

**Veronica Peverelli:** Writing – review & editing, Writing – original draft, Methodology, Investigation, Formal analysis, Conceptualization. **Orlando Sébastien Olivieri:** Writing – review & editing, Investigation, Formal analysis. **Tatsuki Tsujimori:** Writing – review & editing, Resources, Formal analysis. **Donato Giovannelli:** Writing – review & editing, Supervision. **Guanghai Shi:** Resources. **Enrico Cannào:** Writing – review & editing, Formal analysis. **Francesca Piccoli:** Writing – review & editing, Supervision, Formal analysis. **Alberto Vitale Brovarone:** Writing – review & editing, Supervision, Investigation, Funding acquisition, Conceptualization.

## Declaration of competing interest

The authors declare that they have no known competing financial interests or personal relationships that could have appeared to influence the work reported in this paper.

## Acknowledgements

We thank Manuel Menzel and an anonymous reviewer for their constructive feedback, which greatly improved our work. We also thank Ralf Halama and Jeffrey Catalano for careful handling of our manuscript. Our work also benefited from earlier feedback received from Robert M. Hazen and Peter Kelemen. VP and AVB acknowledge Kevin Wong for aiding with preparation of Fig. 5. We thank George Harlow for discussions, Gianluca Sessa for assistance during U–Pb isotope measurements at ESD-UniMi, and Daniela Rubatto for providing the primary RM used for U–Pb isotope measurements at the University of Bern. This work is part of a project funded by the European Research Council (ERC) under the European Union's Horizon 2020 research and innovation program (Grant agreement No. 864045; project acronym DeepSeep). A MIUR Rita Levi Montalcini grant, a MUR FARE grant (No. R20ZIYMPAR; acronym DRYNK), and a MUR PRIN2022 grant (No. 20224YR3AZ; acronym HYDECARB) to AVB are also acknowledged. DG was supported by funding from the European Research Council (ERC) under the European Union's Horizon 2020 research and innovation program (grant number 948972-COEVOLVE-ERC-2020-STG). TT acknowledges funding under grant MEXT/JSPS KAKENHI (JP21H01174).

## Appendix A. Supplementary material

Supplement A contains detailed results of micro-Raman spectroscopy in the form of Raman spectra. It also contains additional information on U–Pb geochronological measurements (Tables S2–S3), particularly on secondary reference materials, and U–Pb isotope data (Tables S4–S6). Supplement B contains on the results of thermodynamic modeling (Table S7) used to construct Fig. 5. Supplement C contains petrographic description of the studied samples. Supplementary material to this article can be found online at <https://doi.org/10.1016/j.gca.2024.10.004>.

## References

- Angiboust, S., Glodny, J., Cambeses, A., Raimondo, T., Monié, P., Popov, M., Garcia-Casco, A., 2021a. Drainage of subduction interface fluids into the forearc mantle evidenced by a pristine jadeite network (Polar Urals). *J. Metam. Geol.* 39, 473–500.
- Angiboust, S., Muñoz-Montecinos, J., Cambeses, A., Raimondo, T., Deldicque, D., Garcia-Casco, A., 2021b. Jolts in the Jade factory: A route for subduction fluids and their implications for mantle wedge seismicity. *Earth Sci. Rev.* 220.
- Barry, P.H., de Moor, J.M., Giovannelli, D., Schrenk, M., Hummer, D.R., Lopez, T., Pratt, C.A., Segura, Y.A., Battaglia, A., Beaudry, P., Bini, G., Cascante, M., d'Errico, G., di Carlo, M., Fattorini, D., Fullerton, K., Gazel, E., González, G., Halldórsson, S.A., Iacovino, K., Ilanko, T., Kulongoski, J.T., Manini, E., Martínez, M., Miller, H., Nakagawa, M., Ono, S., Patwardhan, S., Ramírez, C.J., Regoli, F., Smedile, F., Turner, S., Vetrani, C., Yücel, M., Ballentine, C.J., Fischer, T.P., Hilton, D.R., Lloyd, K.G., 2019. Forearc carbon sink reduces long-term volatile recycling into the mantle. *Nature* 568, 487–492.
- Barry, P.H., De Moor, J.M., Chioldi, A., Aguilera, F., Hudak, M.R., Bekaert, D.V., Turner, S.J., Curtice, J., Seltzer, A.M., Jessen, G.L., Osses, E., Blamey, J.M., Amenábar, M.J., Selci, M., Cascone, M., Bastianoni, A., Nakagawa, M., Filipovich, R., Bustos, E., Schrenk, M.O., Buongiorno, J., Ramírez, C.J., Rogers, T.J., Lloyd, K.G., Giovannelli, D., 2022. The Helium and Carbon Isotope Characteristics of the Andean Convergent Margin. *Front. Earth Sci.* 10, 1–20.
- Bebout, G.E., Penniston-Dorland, S.C., 2016. Fluid and mass transfer at subduction interfaces-The field metamorphic record. *Lithos* 240–243, 228–258.
- Bourg, A.C.M., Loch, J.P.G., 1995. Mobilization of Heavy Metals as Affected by pH and Redox Conditions. In: Salomons, W., Stigliani, W.M. (Eds.), *Biogeochemistry of Pollutants in Soils and Sediments: Risk Assessment of Delayed and Non-Linear Responses*. Environmental Science. Springer, Berlin, Heidelberg, pp. 87–102.
- Boutier, A., Martínez, I., Daniel, I., Tumiat, S., Siron, G., Vitale, A., Min, I.D., 2024a. Computers and Geosciences Thermotopes-COH — A software for carbon isotope modeling and speciation of COH fluids. *Comput. Geosci.* 184, 105533.
- Boutier, A., Martínez, I., Sissmann, O., Agostini, S., Daniel, I., Van Baalen, M., Mana, S., Vitale, B.A., 2024b. Complexity of graphite formation in response to metamorphic methane generation and transformation in an orogenic ultramafic body. *Geochim. Cosmochim. Acta* 364, 166–183.
- Brazelton, W.J., Nelson, B., Schrenk, M.O., 2012. Metagenomic evidence for H<sub>2</sub> oxidation and H<sub>2</sub> production by serpentine-hosted subsurface microbial communities. *Front. Microbiol.* 2, 1–16.
- Brown, M., Johnson, T., 2019. Metamorphism and the evolution of subduction on Earth. *Am. Mineral.* 104, 1065–1082.
- Cesare, B., 1995. Graphite precipitation in C-O-H fluid inclusions: Closed system compositional and density changes, and thermobarometric implications. *Contrib. Mineral. Petrol.* 122, 25–33.
- Chen, A.-X., Chen, X., Chen, Y., Han, X.-Q., Wang, Y.-J., Huang, F., 2023. Low- $\delta^{56}\text{Fe}$  fluid released from serpentine as recorded by iron isotopes of Myanmar jadeites. *Chem. Geol.* 639, 121730.
- Chew, D.M., Petrus, J.A., Kamber, B.S., 2014. U-Pb LA-ICPMS dating using accessory mineral standards with variable common Pb. *Chem. Geol.* 363, 185–199.
- Condie, K.C., Des Marais, D.J., Abbott, D., 2001. Precambrian superplumes and supercontinents: a record in black shales, carbon isotopes, and paleoclimates? *Precamb. Res.* 106, 239–260.
- Connolly, J.A.D., Cesare, B., 1993. C-O-H-S fluid composition and oxygen fugacity in graphitic metapelites. *J. Metam. Geol.* 11, 379–388.
- de Obeso, J.C., Santiago Ramos, D.P., Higgins, J.A., Kelemen, P.B., 2021. A Mg isotopic perspective on the mobility of magnesium during serpentinization and carbonation of the Oman ophiolite. *J. Geophys. Res. Solid Earth* 126, 1–17.
- Dewey, J.F., Kiseeva, E.S., Pearce, J.A., Robb, L.J., 2021. Precambrian tectonic evolution of Earth: an outline. *S. Afr. J. Geol.* 124, 141–162.
- Dilek, Y., 2003. Ophiolite pulses, mantle plumes and orogeny. *Geological Society, London, Special Publications* 218 (1), 9–19.
- Duke, E.F., Rumble, D., 1986. Textural and isotopic variations in graphite from plutonic rocks, South-Central New Hampshire. *Contrib. Mineral. Petrol.* 93, 409–419.
- Etiogo, G., 2023. Massive release of natural hydrogen from a geological seep (Chimaera, Turkey): Gas advection as a proxy of subsurface gas migration and pressurised accumulations. *Int. J. Hydrogen Energy* 48, 9172–9184.
- Fischer, R., Gerya, T., 2016. Regimes of subduction and lithospheric dynamics in the Precambrian: 3D thermomechanical modelling. *Gondw. Res.* 37, 53–70.
- Fu, B., Valley, J.W., Kita, N.T., Spicuzza, M.J., Paton, C., Tsujimori, T., Bröcker, M., Harlow, G.E., 2010. Multiple origins of zircons in jadeite. *Contrib. Mineral. Petrol.* 159, 769–780.
- Fullerton, K.M., Schrenk, M.O., Yücel, M., Manini, E., Basili, M., Rogers, T.J., Fattorini, D., Di Carlo, M., d'Errico, G., Regoli, F., Nakagawa, M., Vetrani, C., Smedile, F., Ramírez, C., Miller, H., Morrison, S.M., Buongiorno, J., Jessen, G.L., Steen, A.D., Martínez, M., de Moor, J.M., Barry, P.H., Giovannelli, D., Lloyd, K.G., 2021. Effect of tectonic processes on biosphere-geosphere feedbacks across a convergent margin. *Nat. Geosci.* 14, 301–306.
- Gerya, T., 2014. Precambrian geodynamics: Concepts and models. *Gondw. Res.* 25, 442–463.
- Giovannelli, D., 2023. Trace metal availability and the evolution of biogeochemistry. *Nat. Rev. Earth Environ.* 4, 597–598.
- Giuliani, A., Drysdale, R.N., Woodhead, J.D., Planavsky, N.J., Phillips, D., Hergt, J., Griffin, W.L., Oesch, S., Dalton, H., Davies, G.R., 2022. Perturbation of the deep-Earth carbon cycle in response to the Cambrian Explosion. *Sci. Adv.* 8, eabj1325.
- Giuntoli, F., Menegon, L., Siron, G., Cognigni, F., Leroux, H., Compagnoni, R., Rossi, M., Vitale, B.A., 2024. Methane-hydrogen-rich fluid migration may trigger seismic failure in subduction zones at forearc depths. *Nat. Commun.* 15, 480.
- Greening, C., Cabotaje, P.R., Alvarado, L.E.V., Leung, P.M., Land, H., Rodrigues-Oliveira, T., Ponce-Toledo, R.I., Senger, M., Klamke, M.A., Milton, M., Lappan, R., Mullen, S., West-Roberts, J., Mao, J., Song, J., Schoelmerich, M., Stairs, C.W., Schleper, C., Grinter, R., Spang, A., Banfield, J.F., Berggren, G., 2024. Minimal and hybrid hydrogenases are active from archaea. *Cell*.
- Griffin, W., Powell, W., Pearson, N.J., O'Reilly, S., 2008. GLITTER: data reduction software for laser ablation ICP-MS. *Short Course Series* 40, 308–311.
- Harada, H., Tsujimori, T., 2024. Methane genesis within olivine-hosted fluid inclusions in dolomitic marble of the Hida Belt, Japan. *Prog. Earth Planet. Sci.* 11, 6.
- Harlow, G.E., 1994. Jadeites, albitites and related rocks from the Motagua Fault Zone, Guatemala. *J. Metam. Geol.* 12, 49–68.
- Harlow, G.E., Sorensen, S.S., 2005. Jade (Nephrite and Jadeite) and Serpentine: Metasomatic Connections. *Int. Geol. Rev.* 47, 113–146.
- Harlow, G.E., Tsujimori, T., Sorensen, S.S., 2015. Jadeites and plate tectonics. *Annu. Rev. Earth Planet. Sci.* 43, 105–138.
- Harlow, G.E., Flores, K.E., Marschall, H.R., 2016. Fluid-mediated mass transfer from a paleosubduction channel to its mantle wedge: Evidence from jadeite and related rocks from the Guatemala Suture Zone. *Lithos* 258–259, 15–36. <https://doi.org/10.1016/j.lithos.2016.04.010>.
- Hay Mele, B., Monticelli, M., Leone, S., Bastoni, D., Barosa, B., Cascone, M., Migliaccio, F., Montemagno, F., Ricciardelli, A., Tonietti, L., Rotundi, A., Cordone, A., Giovannelli, D., 2023. Oxidoreductases and metal cofactors in the functioning of the earth. *Essays Biochem.* 67, 653–670.
- Hazen, R.M., Papineau, D., Bleeker, W., Downs, R.T., Ferry, J.M., McCoy, T.J., Sverjensky, D.A., Yang, H., 2008. Mineral evolution. *Am. Mineral.* 93, 1693–1720.
- Hervieu, C., Verlaque, A., Agard, P., Locatelli, M., Raimbourg, H., Lefeuvre, B., Dubacq, B., 2021. Along-dip variations of subduction fluids: The 30–80 km depth traverse of the Schistes Lustrés complex (Queyras-Monviso, W. Alps). *Lithos* 394–395, 106168.
- Heuer, V.B., Inagaki, F., Morono, Y., Kubo, Y., Spivack, A.J., Viehweger, B., Treude, T., Beulig, F., Schubotz, F., Tonai, S., Bowden, S.A., Cramm, M., Henkel, S., Hirose, T., Homola, K., Hoshino, T., Ijiri, A., Imachi, H., Kamiya, N., Kaneko, M., Lagostina, L., Manners, H., McClelland, H.-L., Metcalfe, K., Okutsu, N., Pan, D., Raudsepp, M.J., Sauvage, J., Tsang, M.-Y., Wang, D.T., Whitaker, E., Yamamoto, Y., Yang, K., Maeda, L., Adhikari, R.R., Glombitza, C., Hamada, Y., Kallmeyer, J., Wendt, J., Wörmer, L., Yamada, Y., Kinoshita, M., Hinrichs, K.-U., 2020. Temperature limits to deep seafloor life in the Nankai Trough subduction zone. *Science* 370, 1230–1234.
- Hirajima, T., 2017. Jadeite and jadeite-bearing rock in the Sanbagawa and the Kamuikotan belts, Japan: A review. *J. Mineral. Petrol. Sci.* 112, 237–246.
- Holder, R.M., Viete, D.R., Brown, M., et al., 2019. Metamorphism and the evolution of plate tectonics. *Nature* 572, 378–381. <https://doi.org/10.1038/s41586-019-1462-2>.
- Holloway, J.R., 1984. Graphite-CH<sub>4</sub>-H<sub>2</sub>O-CO<sub>2</sub> equilibria at low-grade metamorphic conditions. *Geology* 12 (8), 455–458. [https://doi.org/10.1130/0091-7613\(1984\)12<455:GEALMC>2.0.CO;2](https://doi.org/10.1130/0091-7613(1984)12<455:GEALMC>2.0.CO;2).
- Holt, A.F., Condit, C.B., 2021. Slab temperature evolution over the lifetime of a subduction zone. *Geochem. Geophys. Geosyst.* 22.
- Huang, B., Liu, M., Kusky, T.M., et al., 2023. Changes in orogenic style and surface environment recorded in Paleoproterozoic foreland successions. *Nat. Commun.* 14, 7997. <https://doi.org/10.1038/s41467-023-43893-w>.
- Huff, T.A., Nabelek, P.I., 2007. Production of carbonic fluids during metamorphism of graphitic pelites in a collisional orogen-An assessment from fluid inclusions. *Geochim. Cosmochim. Acta* 71, 4997–5015.
- Husson, J.M., Peters, S.E., 2017. Atmospheric oxygenation driven by unsteady growth of the continental sedimentary reservoir. *Earth Planet. Sci. Lett.* 460, 68–75.
- Ingall, E.D., Cappellen, P.V., 1990. Relation between sedimentation rate and burial of organic phosphorus and organic carbon in marine sediments. *Geochim. Cosmochim. Acta* 54, 373–386.
- Johnson, C.A., Harlow, G.E., 1999. Guatemala jadeites and albitites were formed by deuterium-rich serpentinizing fluids deep within a subduction zone. *Geology* 27, 629–632.
- Kelemen, P.B., Carlos de Obeso, J., Leong, J.A., Godard, M., Okazaki, K., Kotowski, A.J., Manning, C.E., Ellison, E.T., Menzel, M.D., Urai, J.L., Hirth, G., Rioux, M., Stockli, D. F., Lafay, R., Beinlich, A.M., Coggon, J.A., Warsi, N.H., Matter, J.M., Teagle, D.A.H., Harris, M., Michibayashi, K., Takazawa, E., Al, S.Z., Kelemen, P., de Obeso, J.C., Matte, J.M., Teagle, D., Coggon, J., Bompard, N., Zihlmann, B., Warsi, N., Harris, M., Morris, T., Bennett, E., Boulanger, M., France, L., Früh-Green, G., Garbe-Schönberg, D., Ildefonse, B., Jesus, A., Manning, C., Mock, D., Müller, S., Noël, J., Nothaft, D., Perez, A., Pezard, P., Zeko, D., 2022. Listvenite formation during mass transfer into the leading edge of the mantle wedge: initial results from Oman drilling project Hole BT1B. *J. Geophys. Res. Solid Earth* 127.
- Kunugiza, K., Goto, A., 2010. Juvenile Japan. Hydrothermal activity of the Hida-Gaien belt indicating initiation of subduction of proto-pacific plate in ca. 520 Ma. *Chigaku Zasshi* 119.
- Leong, J.A., Nielsen, M., McQueen, N., Karolytè, R., Hillemonds, D.J., Ballentine, C., Darrah, T., McGillis, W., Kelemen, P., 2023. H<sub>2</sub> and CH<sub>4</sub> outgassing rates in the Samail ophiolite, Oman: Implications for low-temperature, continental serpentinization rates. *Geochim. Cosmochim. Acta* 347, 1–15.
- Lima-Zaloumis, J., Neubeck, A., Ivarsson, M., Bose, M., Greenberger, R., Templeton, A.S., Czaja, A.D., Kelemen, P.B., Edvinsson, T., 2022. Microbial biosignature preservation in carbonated serpentinite from the Samail Ophiolite, Oman. *Commun. Earth Environ.* 3, 1–11.
- Mangenot, X., Tarantola, A., Mullis, J., Girard, J.P., Le, V.H., Eiler, J.M., 2021. Geochemistry of clumped isotopologues of CH<sub>4</sub> within fluid inclusions in Alpine tectonic quartz fissures. *Earth Planet. Sci. Lett.* 561, 116792.

- Marschall, H.R., Schumacher, J.C., 2012. Arc magmas sourced from mélange diapirs in subduction zones. *Nat. Geosci.* 5, 862–867.
- Meng, F., Makeyev, A.B., Yang, J., 2011. Zircon U-Pb dating of jadeite from the Syum-Keu ultramafic complex, Polar Urals, Russia: Constraints for subduction initiation. *J. Asian Earth Sci.* 42, 596–606.
- Moore, E.K., Jelen, B.I., Giovannelli, D., Raanan, H., Falkowski, P.G., 2017. Metal availability and the expanding network of microbial metabolisms in the Archaean eon. *Nature Geosci.* 10, 629–636.
- Mottl, M.J., Komor, S.C., Fryer, P., Moyer, C.L., 2003. Deep-slab fluids fuel extremophilic Archaea on a Mariana forearc serpentinite mud volcano: Ocean drilling program leg 195. *Geochem. Geophys. Geosyst.* 4, 1–14.
- Müller, R.D., Mather, B., Dutkiewicz, A., Keller, T., Merdith, A., Gonzalez, C.M., Gorczyk, W., Zahirovic, S., 2022. Evolution of Earth's tectonic carbon conveyor belt. *Nature* 605, 629–639.
- Mullis, J., Dubessy, J., Poty, B., O'Neil, J., 1994. Fluid regimes during late stages of a continental collision: Physical, chemical, and stable isotope measurements of fluid inclusions in fissure quartz from a geotraverse through the Central Alps, Switzerland. *Geochim. Cosmochim. Acta* 58, 2239–2267.
- Mullis, J., 1979. The system methane-water as a geologic thermometer and barometer from the external part of the Central Alps. *bullmi* 102, 526–536.
- Neubeck, A., Sun, L., Müller, B., Ivarsson, M., Hosgörmez, H., Özcan, D., Broman, C., Schnürer, A., 2017. Microbial community structure in a serpentine-hosted abiotic gas seepage at the chimaera ophiolite, Turkey. *Appl Environ Microbiol* 83 e03430-16.
- Ohara, Y., Reagan, M.K., Fujikura, K., Watanabe, H., Michibayashi, K., Ishii, T., Stern, R. J., Pujana, L., Martinez, F., Girard, G., Ribeiro, J., Brounce, M., Komori, N., Kino, M., 2012. A serpentine-hosted ecosystem in the Southern Mariana Forearc. *PNAS* 109, 2831–2835.
- Padrón-Navarta, J.A., López, S.-V., Menzel, M.D., Gómez-Pugnaire, M.T., Garrido, C.J., 2023. Mantle wedge oxidation from deserpentinization modulated by sediment-derived fluids. *Nat. Geosci.* 16, 268–275.
- Perchuk, A.L., Zakharov, V.S., Gerya, T.V., Brown, M., 2019. Hotter mantle but colder subduction in the Precambrian: What are the implications? *Precamb. Res.* 330, 20–34.
- Piccoli, F., Hermann, J., Pettke, T., Connolly, J.A.D., Kempf, E.D., Vieira Duarte, D.J., 2019. Subducting serpentinites release reduced, not oxidized, aqueous fluids. *Sci. Rep.* 9, 1–7.
- Piccoli, F., Ague, J.J., Chu, X., Tian, M., Vitale, B.A., 2021. Field-based evidence for intraslab high-permeability channel formation at eclogite-facies conditions during subduction. *Geochem. Geophys. Geosyst.* 22, 1–17.
- Piccoli, F., Rubatto, D., Ovtcharova, M., Hermann, J., Guillong, M., Vitale, B.A., 2023. Dating fluid infiltration and deformation in the subducted ultramafic oceanic lithosphere by perovskite geochronology. *Chem. Geol.* 615.
- Plümpner, O., King, H.E., Geisler, T., Liu, Y., Pabst, S., Savov, I.P., Rost, D., Zack, T., 2017. Subduction zone forearc serpentinites as incubators for deep microbial life. *PNAS* 114, 4324–4329.
- Rempfert, K.R., Miller, H.M., Bompard, N., Nothaft, D., Matter, J.M., Kelemen, P., Fierer, N., Templeton, A.S., 2017. Geological and geochemical constraints on subsurface microbial life in the Samail Ophiolite, Oman. *Front. Microbiol.* 8.
- Stern, R.J., Tsujimori, T., Harlow, G., Groat, L.A., 2013. Plate tectonic gemstones. *Geology* 41 (7), 723–726. <https://doi.org/10.1130/G34204.1>.
- Rogers, T.J., Buongiorno, J., Jessen, G.L., Schrenk, M.O., Fordyce, J.A., de Moor, J.M., Ramírez, C.J., Barry, P.H., Yücel, M., Selci, M., Cordone, A., Giovannelli, D., Lloyd, K.G., 2023. Chemolithoautotroph distributions across the subsurface of a convergent margin. *ISME J.* 17, 140–150.
- Russell, M.J., Hall, A.J., Martin, W., 2010. Serpentinization as a source of energy at the origin of life. *Geobiology* 8, 355–371.
- Schwarzenbach, E.M., Vrijmoed, J.C., Engelmann, J.M., Liesegang, M., Wiechert, U., Rohne, R., Plümpner, O., 2021. Sulfide dissolution and awaruite formation in continental serpentinization environments and its implications to supporting life. *J. Geophys. Res.: Solid Earth* 126.
- Seward, T.M., Williams-Jones, A.E., Migdisov, A.A., 2014. The Chemistry of Metal Transport and Deposition by Ore-Forming Hydrothermal Fluids. Elsevier Ltd.
- Shi, G., Cui, W., Cao, S., Jiang, N., Jian, P., Liu, D., Miao, L., Chu, B., 2008. Ion microprobe zircon U-Pb age and geochemistry of the Myanmar jadeite. *J. Geol. Soc. London* 165, 221–234.
- Shi, G.U., Tropper, P., Cui, W., Tan, J., Wang, C., 2005. Methane (CH<sub>4</sub>)-bearing fluid inclusions in the Myanmar jadeite. *Geochem. J.* 39, 503–516.
- Shock, E.L., 1990. Geochemical constraints on the origin of organic compounds in hydrothermal systems. *Orig. Life Evol. Biosph.* 20, 331–367.
- Sláma, J., Kosler, J., Condon, D.J., Crowley, J.L., Gerdes, A., Hanchar, J.M., Horstwood, M.S.A., Morris, G.A., Nasdala, L., Norberg, N., Schaltegger, U., Schoene, B., Tubrett, M.N., Whitehouse, M.J., 2008. Plešovice zircon - A new natural reference material for U-Pb and Hf isotopic microanalysis. *Chem. Geol.* 249, 1–35.
- Sorensen, S., Harlow, G.E., Rumble, D., 2006. The origin of jadeite-forming subduction-zone fluids: CL-guided SIMS oxygen-isotope and trace-element evidence. *Am. Mineral.* 91, 979–996.
- Spandler, C., Hammerli, J., Sha, P., Hilbert-Wolf, H., Hu, Y., Roberts, E., Schmitz, M., 2016. MKED1: A new titanite standard for in situ analysis of Sm–Nd isotopes and U–Pb geochronology. *Chem. Geol.* 425, 110–126.
- Sperling, E.A., Stockey, R.G., 2018. The temporal and environmental context of early animal evolution: considering all the ingredients of an “Explosion”. *Integr. Comp. Biol.* 58, 605–622.
- Suzuki, N., Koike, K., Kameda, J., Kimura, G., 2024. Thermogenic methane and hydrogen generation in subducted sediments of the Nankai Trough. *Commun. Earth Environ.* 5, 1–10.
- Takahashi, N., Tsujimori, T., Kayama, M., Nishido, H., 2017. Cathodoluminescence petrography of P-type jadeites from the New Idria serpentinite body, California. *J. Mineral. Petrol. Sci.* 112, 291–299.
- Takahashi, N., Tsujimori, T., Chang, Q., Kimura, J.-I., 2018. *In-situ* lithium isotope geochemistry for a veined jadeite from the New Idria serpentinite body, California: Constraints on slab-derived fluid and fluid-rock interaction. *Lithos* 318–319, 376–385.
- Takai, K., Nakamura, K., Toki, T., Tsunogai, U., Miyazaki, M., Miyazaki, J., Hirayama, H., Nakagawa, S., Nunoura, T., Horikoshi, K., 2008. Cell proliferation at 122°C and isotopically heavy CH<sub>4</sub> production by a hyperthermophilic methanogen under high-pressure cultivation. *PNAS* 105, 10949–10954.
- Tao, R., Zhang, L., Tian, M., Zhu, J., Liu, X., Liu, J., Höfer, H.E., Stagno, V., Fei, Y., 2018. Formation of abiotic hydrocarbon from reduction of carbonate in subduction zones: Constraints from petrological observation and experimental simulation. *Geochim. Cosmochim. Acta* 239, 390–408.
- Truttschel, L.R., Kruger, B.R., Sackett, J.D., Chadwick, G.L., Rowe, A.R., 2023. Determining resident microbial community members and their correlations with geochemistry in a serpentinizing spring. *Front. Microbiol.* 14.
- Tsujimori, T., 2017. Early Paleozoic jadeites in Japan: An overview. *J. Mineral. Petrol. Sci.* 112, 217–226.
- Tsujimori, T., Harlow, G.E., 2012. Petrogenetic relationships between jadeite and associated high-pressure and low-temperature metamorphic rocks in worldwide jadeite localities: a review. *Eur. J. Mineral.* 24, 371–390.
- Tsujimori, T., Harlow, G.E., 2017. Jadeite (jadeite jade) from Japan: History, characteristics, and perspectives. *J. Mineral. Petrol. Sci.* 112, 184–196.
- Tsujimori, T., Itaya, T., 1999. Blueschist-facies metamorphism during Paleozoic orogeny in southwestern Japan: Phengite K-Ar ages of blueschist-facies tectonic blocks in a serpentine mélange beneath early Paleozoic Oeyama ophiolite. *Isl. Arc* 8, 190–205.
- Tsujimori, T., Liou, J.G., Wooden, J., Miyamoto, T., 2005. U-Pb dating of large zircons in low-temperature jadeite from the osayama serpentinite Mélange, Southwest Japan: insights into the timing of serpentinization. *Int. Geol. Rev.* 47, 1048–1057.
- Upin, H.E., Newell, D.L., Colman, D.R., Boyd, E.S., 2023. Tectonic settings influence the geochemical and microbial diversity of Peru hot springs. *Commun. Earth Environ.* 4, 1–8.
- Van Keken, P.E., Hacker, B.R., Syracuse, E.M., Abers, G.A., 2011. Subduction factory: 4. Depth-dependent flux of H<sub>2</sub>O from subducting slabs worldwide. *J. Geophys. Res.: Solid Earth* 116.
- Vermeesch, P., 2018. IsoplotR: A free and open toolbox for geochronology. *Geosci. Front.* 9, 1479–1493.
- Vitale, Brovarone, A., Sverjensky, D.A., Piccoli, F., Ressico, F., Giovannelli, D., Daniel, I., 2020. Subduction hides high-pressure sources of energy that may feed the deep subsurface biosphere. *Nat. Commun.* 11, 1–11.
- Walton, C.R., Hao, J., Huang, F., Jenner, F.E., Williams, H., Zerkle, A.L., Lipp, A., Hazen, R.M., Peters, S.E., Shorttle, O., 2023. Evolution of the crustal phosphorus reservoir. *Sci. Adv.* 9, eade6923.
- Walton, C.R., Shorttle, O., 2024. Phanerozoic biological reworking of the continental carbonate rock reservoir. *Earth Planet. Sci. Lett.* 632, 118640.
- Wen, J., Shi, G., Xing, B., Long, T., Zhang, J., 2023. Unique interstitial textures within coarse-grained jadeite from Kazakhstan and their significance in locality identification. *Minerals* 13.
- Wiedenbeck, M., Allé, P., Corfu, F., Griffin, W. I., Meier, M., Oberli, F., Quadt, A. V., Roddick, J. C., Spiegel, W., 1995. Three Natural Zircon Standards for U-Th-Pb, Lu-Hf, Trace Element and Re Analyses. *Geostandards Newsletter* 19, 1–23.
- Wiedenbeck M., Hanchar J. M., Peck W. H., Sylvester P., Valley J., Whitehouse M., Kronz A., Morishita Y., Nasdala L., Fiebig J., Franchi I., Girard J.-P., Greenwood R. c., Hinton R., Kita N., Mason P. r. d., Norman M., Ogasawara M., Piccoli P. m., Rhede D., Satoh H., Schulz-Dobrick B., Skår O., Spicuzza Mj., Terada K., Tindle A., Togashi S., Vennemann T., Xie Q. and Zheng Y.-F., 2004. Further Characterisation of the 91500 Zircon Crystal. *Geostandards Geoanal. Res.*, 28, 9–39.
- Wilson, C.R., Spiegelman, M., van Keken, P.E., Hacker, B.R., 2014. Fluid flow in subduction zones: The role of solid rheology and compaction pressure. *Earth Planet. Sci. Lett.* 401, 261–274.
- Woycheese, K.M., Meyer-Dombard, D.R., Cardace, D., Argayosa, A.M., Arcilla, C.A., 2015. Out of the dark: Transitional subsurface-to-surface microbial diversity in a terrestrial serpentinizing seep (Manleluag, Pangasinan, the Philippines). *Front. Microbiol.* 6, 1–12.
- Yanagawa, K., Ijiri, A., Breuker, A., Sakai, S., Miyoshi, Y., Kawagucci, S., Noguchi, T., Hirai, M., Schippers, A., Ishibashi, J., Takaki, Y., Sunamura, M., Urabe, T., Nunoura, T., Takai, K., 2017. Defining boundaries for the distribution of microbial communities beneath the sediment-buried, hydrothermally active seafloor. *ISME J.* 11, 529–542.
- Yui, T.F., Maki, K., Usuki, T., Lan, C.Y., Martens, U., Wu, C.M., Wu, T.W., Liou, J.G., 2010. Genesis of Guatemala jadeite and related fluid characteristics: Insight from zircon. *Chem. Geol.* 270, 45–55.
- Zerkle, A.L., 2018. Biogeodynamics: Bridging the gap between surface and deep Earth processes. *Philosophical Transactions of the Royal Society a: Mathematical, Physical and Engineering Sciences* 376.